BioCore Exploring Scientific Community

International Journal of Nanotechnology in Medicine & Engineering

ISSN 2474-8811

Research Article Open Access

Synthesis and Characterization of Cellulose Nanoparticles and its Derivatives using a Combination of Spectro-Analytical Techniques

Yakubu Azeh*[1], Gabriel Ademola Olatunji[2], Folahan Amoo Adekola[2]

[1]Department of Chemistry, Ibrahim Badamasi Babangida University, Lapai, Niger State, Nigeria

[2]Department of Industrial Chemistry, University of Ilorin, Ilorin, Nigeria

Corresponding Author: Yakubu Azeh, Department of Chemistry, Ibrahim Badamasi Babangida University, Lapai, Niger State, Nigeria. **Email:** yakubuazeh@gmail.com

Citation: Yakubu Azeh et al. (2017), Synthesis and Characterization of Cellulose Nanoparticles and its Derivatives using a Combination of Spectro-Analytical Techniques. Int J Nano Med & Eng. 2:6, 64-91. DOI:10.25141/2474-8811-2017-6.0065

Received: April 20, 2017; **Accepted:** May 01 2017; **Published:** July 06, 2017

Abstract:

Nanoparticles from different cellulosic sources were prepared via hydrolysis using three different acids. Cellulose, Methylcellulose (MC), Cellulose acetate (CA), Propylcellulose (PC) and Ethylcellulose (EC) was hydrolyzed using pulp-to-liquid ratio of 4.57:1 under 1/3/6 h hydrolysis. Different particles ranging from 70 - 1580 nm were obtained. The maximum yield (55.3 %) was attained at 3 h hydrolysis with H3PO4 acid, and particle size decreased with increasing reaction time as revealed by SEM and fiber length histograms and BET. Most fibers had pore area around 0.41 µm2. Nanoparticles obtained from all cellulose derivative used had low crystallinity index value attributed to substituent groups. The TGA showed that the prepared nanoparticles have thermal stability at T95 and T90 (5 and 10 wt % mass loss) in the temperature range of 297.51-411.09 oC and 315-508.55 oC with Tmax, 375-525 oC respectively. An extended temperature range was observed for some samples over the whole temperature range with only 50 wt % mass loss of the nanomaterials. FT-IR spectroscopy was employed to study the characteristic functionalities found in crystalline cellulose. BET analysis of samples gave evidences of the nanoparticles possessing large surface area of between 105.698 m2/g and 250.570 m2/g. The Langmuir surface area was 10336.157 m2/g, while the pore size and pore volume, ranged from 1.324 – 9.237 nm and 0.01427 – 0.07939 cm3/g respectively. The three different acids used gave various yields of nanocrystals with H3PO4 having the highest yield of 55.3 %, followed by HCl, (34.8 %) while H2SO4 has the lowest yield of 30 %. All of these yields were obtained under the same reaction conditions during 3 h hydrolysis. All samples hydrolyzed for 6 h gave low yield, 28.2 % of nanoparticles. The 3 h hydrolysis was the optimum reaction time for the generation of nanoparticles using 4.57 mL/g solid-liquid ratio.

Keywords: Cellulose Nanocrystals, Acid Hydrolysis, SEM, FT-IR, XRD, TGA, BET

Introduction:

Cellulose is a linear biopolymer consisting of alternating amorphous and crystalline domains of D-anhydroglucopyranose units linked together by β1→4-glycosidic bonds, resulting in bundles known as microfibrils that can be easily cleaved by mineral acids (Rodionova, Lenes, Eriksen and Gregersen 2010; Azeh, Umar and Mohammed 2011; Koroleva, Huebner, Lukanina, Khvatov, Popov and Monakhova 2012; Yanxia, Tiina, Carlos, Julio, Ingrid and Orlando 2013). Cellulose is the most predominant basic structural components of all plant fibres and the most important organic and renewable biopolymer produced by plants worldwide (Atanu, Badal, John, Shogren and Willett 2006; Sercer, Raos and Rujnic-Sokele, 2009; Dieter, Schmauder, Thomas 2011; Peng, Dhar, Liu and Tam 2011; Jonas 2014; Yanxia et al. 2013). It is a biodegradable and non-toxic biopolymer (Peng et al. (2011). It is a versatile starting material for the production of value-added products such as, cellulose-based threads and films as well as a variety of stable cellulose derivatives used in many areas of industry and domestic life (Atanu et al. 2006; Olatunji 2009).

Derivatizing cellulose interferes with the orderly crystal-forming hydrogen bonding, so that even hydrophobic derivatives may increase the apparent solubility in water. Methylcellulose,

Cellulose acetate, Ethylcellulose, Carboxymethylcellulose and native cellulose have been used in various industrial applications and these include; barriers films, thickener and emulsifier, lubricant, glue and binder, artificial tears and saliva, optical and biomedical devices, pharmaceutical raw materials, flame retardants, resins and filters, blends and composites. Because of their low cost, toughness, natural feel, transparency, softness, comfort and other favourable aesthetic properties (Rodionova et al. 2009; Jering and Gunther 2010; Azeh et al. 2011; Koroleva, Huebner, Lukanina, Khvatov, Popov and Monakhova 2012; Zhang, Nypelo, Salas, Arboleda, Hoeger and Rojas 2013; Xavier 2014). Carbohybrid composites, cellulose and nanocellulose-hydroxyappatite composites for bone and tissue regeneration, and templates for bio-imaging and pH sensing applications have been synthesized (Saska, Barud, Gaspar, Marchetto, Ribeiro and Messaddeq 2011; Basu, Sharan, Kumar and Manjubala 2014).

Nanocrystalline cellulose is the individual nanocrystalline regions of elementary nanofibrils of crystalline cellulose obtained after the amorphous regions have been removed via hydrolysis with strong acids with their particle size depending on temperature, acid concentration and time (Rodionova et al. 2010; Koroleva et al. 2012; Yanxia et al. 2013). Nanocrystalline cellulose in the range of 100–300 nm long have been isolated and it is anywhere from a tenth to a quarter of the strength of carbon Nanotubes (Marthin, Orlando, Lucian and Mohini (2008). The incorporation of only a few percent of these cellulosic nanomaterials normally (1–5 %) into a polymer matrix can lead to vast improvements due to their large degree of surface area, stiffness, strength, toughness, thermal stability, barrier properties and flame retardancy compared to the pure polymer matrix (Stephen (2010). Because of the nanometric size effect, composites from these materials show some unique and outstanding properties with respect to their conventional microcomposites counterparts. Since the pioneering work by the Toyota group according to Robert et al. (2011), polymer nanocomposites have attracted much more attention, particularly; the incorporation of nanoscale materials into conventional polymer matrices has created a broad range of materials with novel applications. These advantages are mainly derived from their high aspect ratio, high interfacial area and their extent of dispersion and percolation, which takes place when the nano filler particles start physically interacting, forming a continuous network due to large surface area for contact; greater fraction of atoms are exposed on the surface, and a high surface to volume ratio in contrast to their bulk counterparts (Stephen 2010; Tsagaye 2012). A decreased in the size of a nanoparticle leads to a fractional increase in the surface atoms and consequently, it increases reactivity and makes them highly reactive. Nanodimensional cellulose has already been used as a template to produce electrical wires of various metals through electroless deposition (Robert et al. (2011). Cellulose and cellulose nanocomposites for self-cleaning textiles as well as solar cell, biosensors and electronic storage devices have also been documented (Baptista, Ferreira and Borges, 2013; Ricardo, Marcia, Carlos and Tito 2012). Cadmium sulphide (CdS) nanowire has been made using a nanocellulose derivative (Lucian and Orlando 2009; Robert et al. 2011; Haorna et al. 2014). Other applications could be possible if one were able to combine other inorganics with cellulose as reported by Lucian and Orlando (2009). Cellulose has also been used for electrical devices (including artificial muscles), due to its piezoelectric nature Lucian and Orlando (2009). Smart cellulose/ electroactive paper (EAPap), a chemically treated paper with thin electrodes has been reported. Cellulose nanocrystals can be used as a starting material for the next generation of cellulose based materials of high mechanical strength, toughness, load bearing potentials, light weight, low density, low cost, biodegradability, enhanced energy recovery and chemical property stability (Robert et al. (2011). Under careful selection of reaction conditions, highly crystalline rod-like hydrophilic cellulose nanocrystals with properties comparable to other nano reinforcement materials can be obtained (Robert et al. 2011; Filpponen 2009). Cellulose nanocrystals have low cost compared to other nanoparticles and have high aspect ratio (length/diameter) varying between 30 – 150 depending on the source and processing method from which it is obtained (Robert et al. 2011; Filpponen 2009). Nanocellulose has low density (1.6 g cm-3) and reactive surfaces of hydroxyl (–OH) sites which facilitates surface functionalization through grafting and click reactions to achieve various modifications with different surface properties. Some variety of CN composites produced to date can be, transparent, have tensile strengths greater than cast iron, and have very low coefficient of thermal expansion (LCTE). Besides them being relatively cheap and biodegradable materials, are their competitive mechanical properties. For example, cellulose nanocrystals have been reported to be stronger than steel and stiffer than aluminum. The elastic modulus and tensile strength have been reported to be 145 GPa and 7.5 GPa (Robert et al. 2011; Filpponen 2009; Kuga and Brown, 1987).

Potential applications include but not limited to barrier films, antimicrobial films, transparent films and flexible displays, reinforcing fillers for polymers, biomedical implants, pharmaceuticals, drug delivery, fibers and textiles, templates for electronic components, separation membranes, batteries, super capacitors, electroactive polymers, development of magnetic materials for data storage, optoelectronics, medical diagnostics, photo-catalysts, sensors, alternative energy, communications, water purification, pollution reduction, medical and biomedical applications and many more (Robert et al. 2011; Jonas 2014; Tsegaye 2012; Haoran et al. 2014). Nanocrystalline cellulose materials have been used as strong template for impregnation of a range of different nanomaterials to form composites. For example, metals (Au, Ag, Pd, Ni, etc.), mineral (Cax(PO4)y, CaCO3 and montmorillonite), and carbon (carbon nanotube and graphene) nanomaterials have been incorporated into nanocellulose, and materials with extraordinary electrical, optical and catalytic properties were obtained (Haoran et al. 2014). The objective of this paper was to discuss the results of synthesis of cellulose nanoparticles from cellulose, methylcellulose, cellulose acetate and ethylcellulose by acid hydrolysis and to also determine the optimum conditions for the reaction. The products synthesized were then characterized in relation to their morphologies by SEM,

FT-IR, TGA, BET and XRD.

Experimental Methods:

Materials:

All the chemicals used in the synthesis of nanocellulose and its derivatives were of analytical grade and obtained from BDH Chemicals Ltd (Poole England). They were used without any further purification and these include; Cellulose, Cellulose acetate, Methylcellulose, Ethylcellulose, Propylcellulose and concentrated H2SO4, HCl and H3PO4.

Synthesis and Purification of Cellulosic Nanocrystals (CNCs):

The preparation of cellulose nanocrystals followed the procedures described by (Filpponen 2009; Rosa et al. 2010; Jabbar and Timell 1960). In a typical experiment, 1 gram each of the cellulosic source material was hydrolyzed using 40 mL 64 % (4.57 mL/g) concentrated H2SO4, HCl and H3PO4 at 50 oC for 3/6 h under continuous mechanical stirring with a Teflon coated magnetic bar. The resulting suspension obtained had different colours depending on hydrolysis time. The obtained viscous suspension was neutralized using distilled water and then centrifuged at 3000 rpm for 30 min. and then washing was repeatedly carried out using centrifugation until the nanoparticle obtained was neutral. The thoroughly washed products were then kept in suspension by the addition of deionized water in plastic sample bottles and then stored in a refrigerator. These samples were used for SEM, XRD and surface area analysis. Soluble products obtained were allowed to stand to precipitate overnight. Methylated cellulose nanocrystals were obtained as hydrogels by salting out. All the products obtained were assigned codes as shown in the table below:

Table 1: Sample Codes for Hydrolysis

Sample/Acid		
AZH1/CELL/H_2SO_4	AZH2/CA/H_2SO_4	AZH3/CELL/HCl
AZH4/CA/HCl	AZH5/MC/H_2SO_4	AZH6/MC/HCl
AZH7/CELL/H_3PO_4	AZH8/CA/H_3PO_4	AZH9/EC/H_2SO_4
AZH10/CELL/H_3PO_4	AZH11/CA/H_3PO_4	AZH/MC/H_3PO_4

Scanning Electron Microscopy:

The surface morphology of the samples was carried out using PhenomWorld ProX desktop scanning electron microscope with fully integrated and specifically designed EDS detector made in Eindhoven Netherlands.

FT-IR results of Cellulose, Methylcellulose and Cellulose acetate nanoparticles:

The FT-IR spectra of samples were recorded FT-IR-8400S Fourier Transform Infrared

Spectrophotometer in the spectra range of 4000-400 cm-1. Samples were run as (Kbr) pellets,

X-Ray Diffraction (XRD) Analysis of samples:

X-ray diffractometry in reflection mode was carried out using a diffractometer (DLMAX-2550, Japan), with monochromatic Cu Kα radiation (λ = 0.154 nm), with a divergence and scatter at 1.00o, and a receiving slits at 0.30 mm, generated at 40 kV and 30 mA, at room temperature. The samples were scanned within 2.00 - 70.00˚ 2θ in continuous scan mode with a step of 0.02˚ and a rate of 0.10 sec. The crystallite index of cellulose was calculated using the Kim's empirical method.

$$\mathbf{CI = (I002\text{-}Iam)/I002 \times 100}$$

Where CI is the crystallinity index, I002 is the maximum intensity and represents crystalline material, while Iam represents maximum intensity of the amorphous material.

Thermogravimetric Analysis (TGA):

Thermal behaviour of the prepared samples was examined by Thermogravimetric Analyzer model Schimadzu TGA-50H (Kyoto, Japan) from 28 °C to 900 °C. A heating rate of the analysis was 10 °C / min under nitrogen atmosphere and at a flow rate of 20 mL / min.

BET Analysis:

The surface area of the prepared samples was examined by BET analysis using Quantachrome NovaWin-Data Acquisition and Reduction for NOVA instruments version 11.03.

Results and Discussion:

Appearance of nanoparticle solutions/suspensions:

The appearances of nanoparticle solutions/suspension obtained were in agreement with other documented works on different techniques for the synthesis of nanoparticles from cellulose, methylcellulose, cellulose acetate and ethylcellulose sources and other agricultural wastes (Vipuls and Swapan 2012; Hong et al. 2012; Youssef et al. 2010).

Table 2: Effect of hydrolysis condition on the appearance of nanoparticles solution/suspension (Vipuls and Swapan 2012; Amit 2013; Youssef et al. 2010)

S/No	Sample/Acid	Reaction Temperature (°C)	Reaction Time (min)	Appearance of the suspension
1	AZH1/CELL/H_2SO_4	50	180	Dark-brown cellulose suspension, viscous
2	AZH2/CA/H_2SO_4	50	180	Dark-brown cellulose acetate suspension, viscous
3	AZH3/CELL/HCl	50	180	Ivory white-milky suspension, viscous
4	AZH4/CA/HCl	50	180	Ivory white-milky solution, viscous
5	AZH5/MC/H_2SO_4	50	180	Dark-brown solution
6	AZH6/MC/HCl	50	180	White milky solution, viscous
7	AZH7/CELL/H_3PO_4	50	180	Ivory white milky suspension, viscous
8	AZH8/CA/H_3PO_4	50	180	Clear solution, viscous
9	AZH9/EC/H_2SO_4	50	180	Dark-brown solution
10	AZH10/CELL/H_3PO_4	50	360	White milky suspension, viscous
11	AZH11/CA/H_3PO_4	50	360	White milky suspension, viscous
12	AZH/MC/H_3PO_4	50	60	Clear solution, viscous

Table 3: Experimental conditions: Reaction time and acid-to-pulp ratios

S/No	Sample/Acid	Reaction Temperature (^{0}C)	Reaction Time (min)	Liquid-to-Solid Ratios based on 4.57 mL/g
1	AZH1/CELL-/H_2SO_4	50	180	4.57:1
2	AZH2/CA/H_2SO_4	50	180	4.57:1
3	AZH3/CELL/HCl	50	180	4.57:1
4	AZH4/CA/HCl	50	180	4.57:1
5	AZH5/MC/H_2SO_4	50	180	4.57:1
6	AZH6/MC/HCl	50	180	4.57:1
7	AZH7/CELL/H_3PO_4	50	180	4.57:1
8	AZH8/CA/H_3PO_4	50	180	4.57:1
9	AZH9/EC/H_2SO_4	50	180	4.57:1
10	AZH10/CELL/H_3PO_4	50	360	4.57:1
11	AZH/MC/H_3PO_4	50	60	4.57:1
12	AZH/CA/H_3PO_4	50	360	4.57:1

Morphological Properties Of Samples:

SEM Micrographs of 3h/H2SO4 hydrolyzed Samples

The SEM images of the samples AZH1-CELL-3h-H2SO4, AZH2-CA-3h-H2SO4 and AZH5-MC-3h-H2SO4 hydrolyzed under the same reaction conditions showed clear evidences of the absence of elongated fiber and bundles of cellulose, CA and MC due to hydrolysis Figures A.1-A.3. The presence of different crystalline sizes with irregular shapes of single and agglomerated particles with sharp edges having length ranging from 69.89 – 838.89 nm with few ranging from several nano meters to micrometer scale can be seen in the micrographs at different magnifications Figure A.1. Nanoparticle-rods of cellulose acetate were isolated and were homogenously distributed with a stream-like configuration (Zhong-Yan et al. (2011). The images revealed the presence of large block-like crystalline aggregated nanoparticles of various sizes and shapes on the surface with sharp corner edges and bright spots (Figure A.4) similar to the work described by Vipuls and Swapan (2012). Evidence of interconnected web-like structures of tiny nanofibrils, and fissured porous surface was also observed. Nanoparticles ranging from 132 nm – 1580 nm were isolated Figure A.5. At higher magnification, the presence of rod-like and /or needle-like nanoparticles was visibly clear on the surface of the clusters of the various fragments and agglomerates for the MC nanoparticles Figure A.21. There was also, good evidence

of interconnected web-like structures. SEM images revealed acid diffusion process into the morphology of MC which showed the formation of rod-like individual crystallite due to subsequent release of amorphous regions (Susheel et al. 2011; Allain 2013). Structures of this type have been reported with fiber diameter of 20 nm – 800 nm (Denis et al. 2011; Xiaoyun and Shuwen 2013). The fiber length distribution intensity showed that high number of fiber particles were in nanometer scale and ranging from 86 nm – 1040 nm equivalence of 0.086 µm – 1.04 µm Figure A.11. Cellulose nanocrystals isolated resembles those reported by Vipuls and Swapan (2012) Figure A.1. SEM images of these three cellulosic materials also revealed the roughness of the surface porosity of the particles which is not found in native materials. The fiber metric histogram showed the percent intensity of fiber length distribution frequency and it showed that a high fraction of the fibers were in nano scale. Nanocellulose whiskers with length in range of 100-600 nm, 250-270 nm and approximately 500 nm with 10 nm in diameter prepared using 63.5 % H2SO4/2 h hydrolysis have been reported by (Amit 2013; Hong et al. 2012; Youssef et al. 2010) Figure A.2. Cellulose whiskers with 6.88 µm length isolated under 120 min at acid concentration of 44.1 % at 80 oC and 10 min ultrasonication have been reported (Amit, 2013). A random analysis of the pore area measurement of the nanoparticles indicated that most of the fibers had pore area distribution ranging from 41000 - 82000 nm2 Figure A.2-A.3, A.5-A.6, A.8-A.9. The implication of the synthesized nanoparticles is that the presence of the large surface area will aid the encapsulation and homogenous distribution of conventional adsorbents for improved performance. The pore area histogram, which is very important in revealing the frequency of average pore volume, is essential for pore size applications in filtration. The liquid-to-solid ratio in this work was 4.57:1 (4.57 mL/g) in contrast to most reports on cellulose nanocrystals employing liquid-to-solid (mL/g) ratio of 8.75:1 (8.75 mL/g) in the determination of sulphur contents in cellulose nanocrystals at various liquid-to-solid ratio and time Amit (2013). The implication is that, the generation of nanocellulose crystals is time, temperature and acid concentration dependant. The MC nanoparticles were larger than cellulose nanocrystals.

The pore area of the MC nanoparticles was much greater than that for the cellulose nanoparticles and the acetate nanoparticles. The nanocellulose crystals had smaller particles with high porosity than those obtained from cellulose acetate fibers. The reason for the large size and low pore area of the nanoparticles from the acetate derivative could be due to the presence of acetyl group`s resistance to acid attack. The pore size and fiber diameter of these particles can be beneficial for cleaning applications such as for the removal of organic pollutants in water systems.

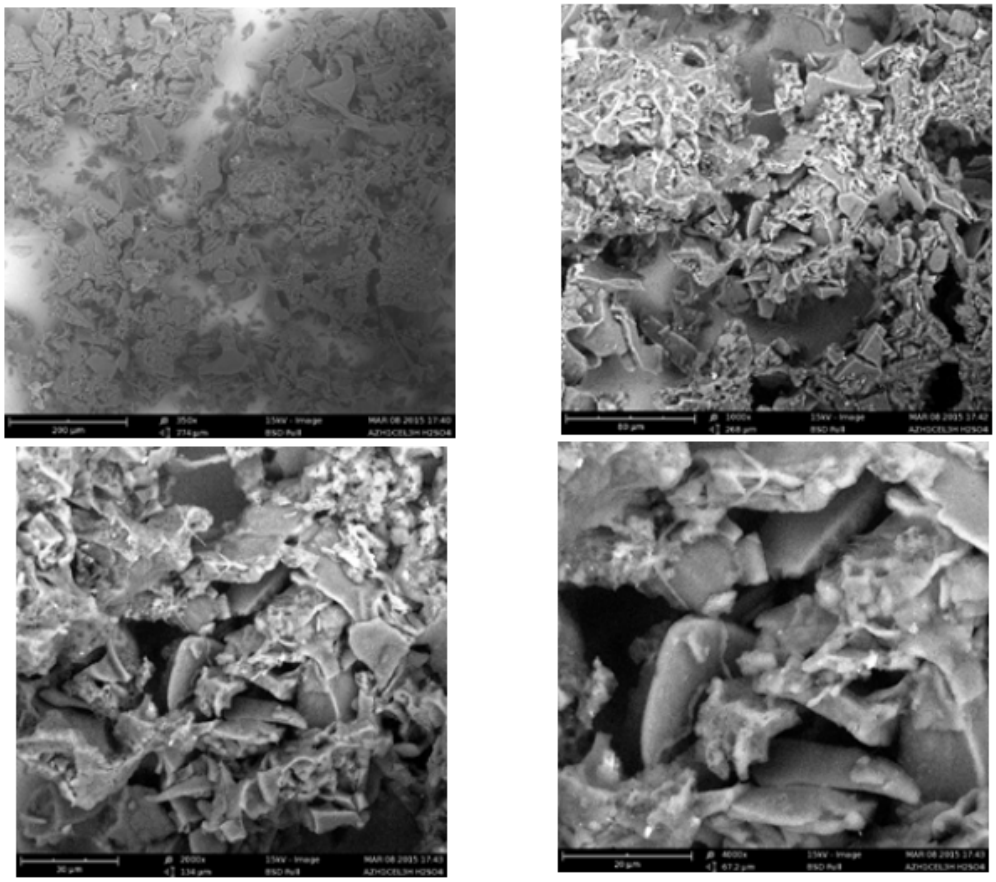

Fig. A.1: SEM Micrographs of AZH1-3h-CELL-H2SO4

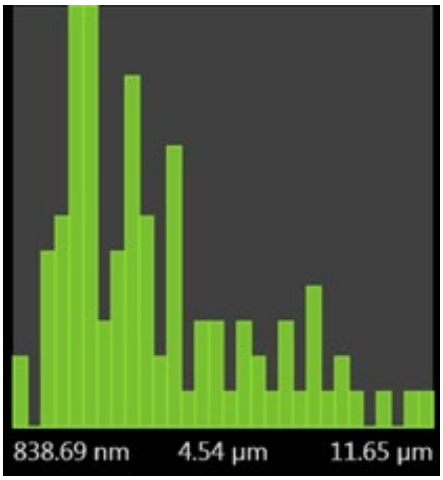

Fig. A.2: Fiber Length Histogram

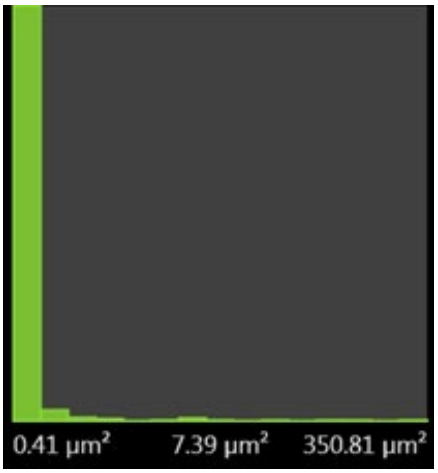

Fig. A.3: Fiber Pore Area Histogram

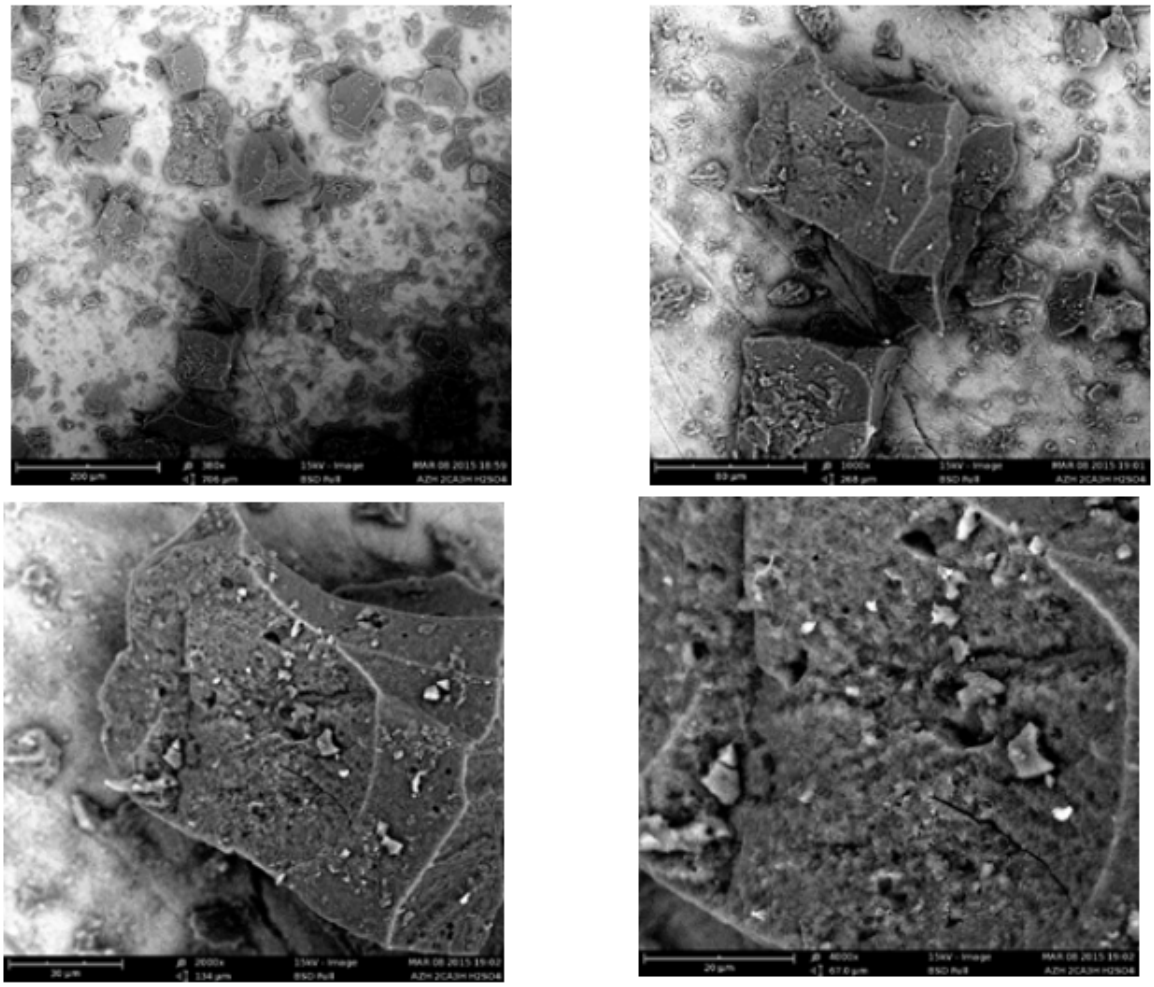

Fig. A.4: SEM Image of AZH2-CA-3h-H2SO4

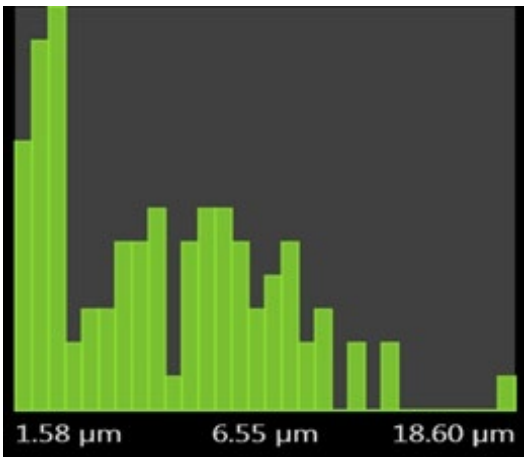

Fig. A.5: Fiber Length Metric Histogram

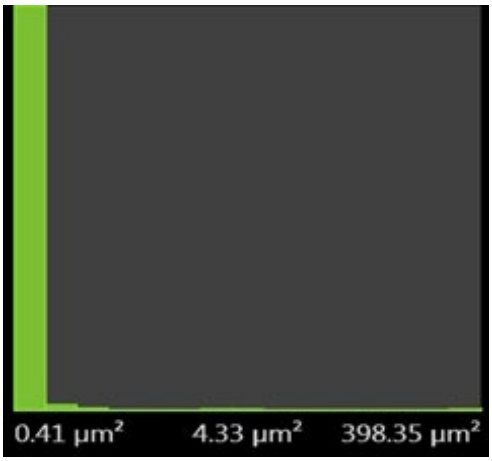

Fig. A.6: Pore Fiber Area Histogram

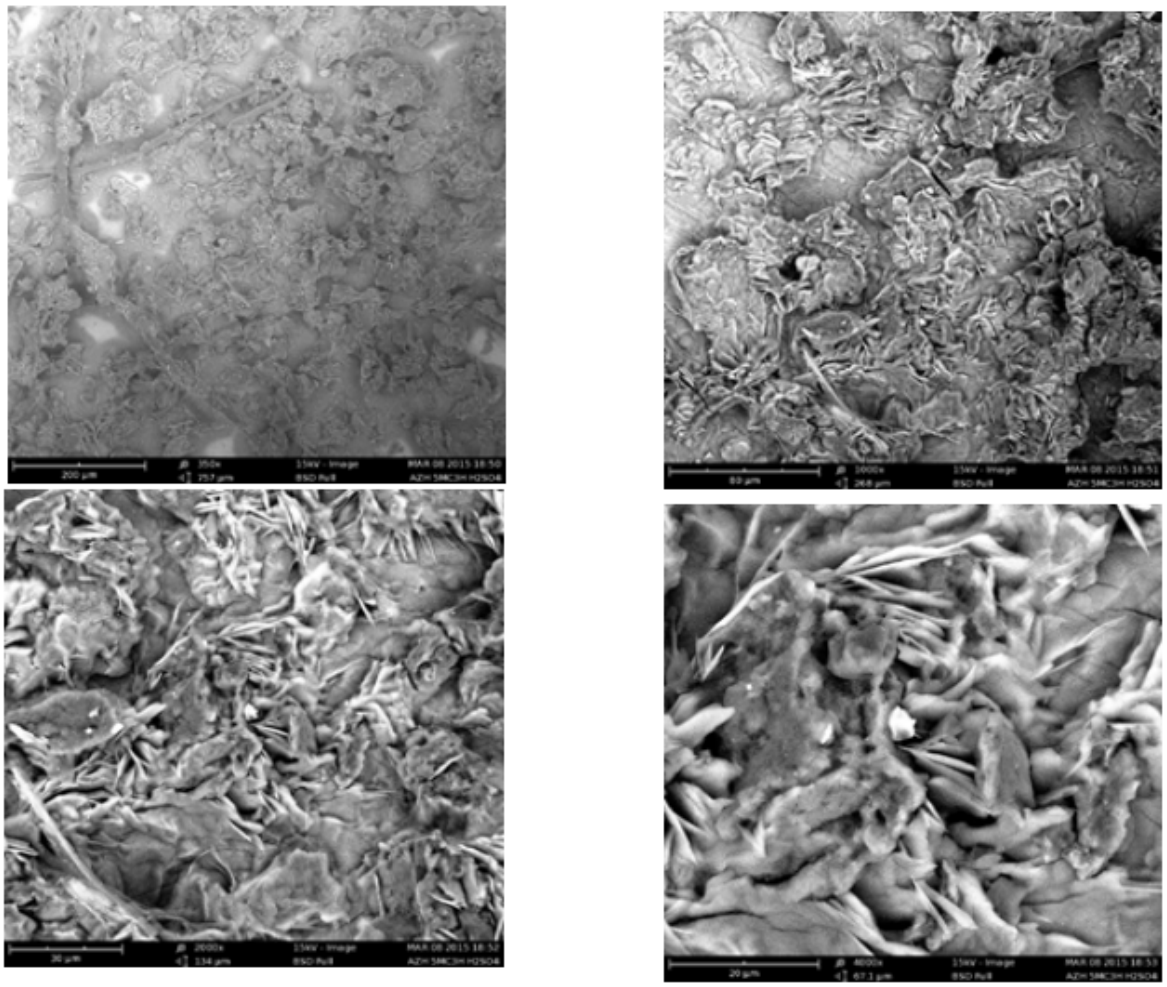

Fig. A.7: SEM Image of AZH5-MC-3h-H2SO4

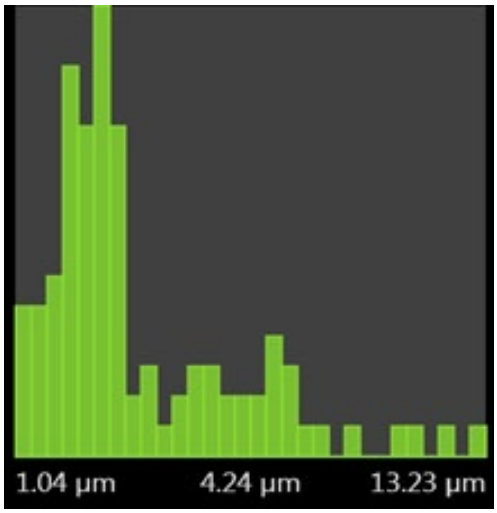

Fig. A.8: Fiber Length Histogram

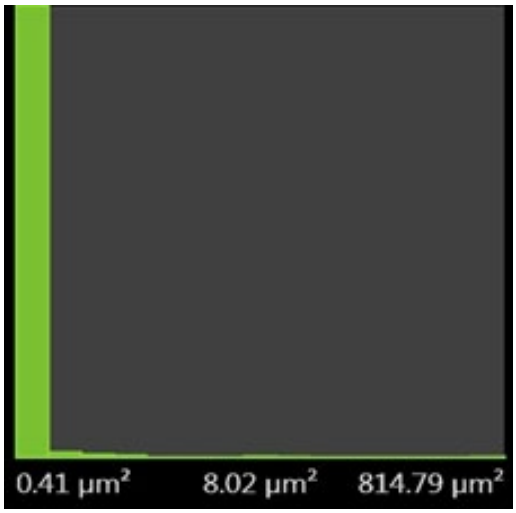

Fig. A.9: Fiber Pore Area Histogram

1.10.2 SEM Micrographs of 3/6h/HCl hydrolyzed Samples:

The 3 h acid degradation of cellulose and MC fibers using 64 % HCl caused a breakdown of the cellulose fiber into short microcrystals which formed agglomerates of various sizes Figure A.10 below. While AZH6-MC-3h-HCl (Figure A.16) showed the presence of individual crystallites which appeared as white spot. Also seen in the MC particles, were the appearance of rod-like nanoparticles. These are clear evidences of degradation of the amorphous portions in cellulose and MC fibers. The various agglomerations, fragments and web-like interconnected structures observed are similar to those synthesized using a mixture of HCl-H2SO4 solution. These features are all attributed to the formation of hydroxylated surfaces due to hydrogen bonding Michaela (2013). The absence of long cellulose fiber bundles was observed for both samples, and is due to the reaction time for hydrolysis. The structures of native cellulose fibers have been revealed to have very long fibrils which collect into bundles as demonstrated by several works on cellulose blends and composites (Zhong-Yan et al. 2011; Yakubu et al. 2012). The fiber length distribution intensity for nanocellulose particle was indicative of the presence of majority of the fibers with length of 263 nm (Youssef et al. 2010; Denis et al. 2011; Susheel et al. 2011; Amit 2013). While the SEM micrographs of AZH4-CA-3h-HCl (Figure A.13) showed the formation of a homogenous phase of individual rod-like crystals. Various shapes and sizes of agglomerated crystalline particles with a close packing and interconnected web-like network was revealed on the surface of the nanoparticles at higher magnification as reported by Zhong-Yan et al. (2011) Figure A.16 below. These structural properties can be useful for application in the preparation of high strength composites, filtration of large organic and inorganic materials etc. Nanocellulose particles with 82 nm fiber length were prepared. Fibers with length ranging from 6.91 µm – 19.09 µm micrometers were also detected (Yussef et al. 2010; Susheel et al. 2011). The pore area of the particles showed that a high fraction of the fibers had size within 0.082 µm2 which is equivalent to 82000 nm2 with the highest frequency distribution count. This particles exhibited high kinks and homogenous surface area that is not found in cellulose acetate. This property can be apply for the removal of large organic molecules in waste and polluted water due to their small size. The presence of acetyl groups will necessitate hydrophobic interactions with organic molecules thus, enabling their removal in polluted and waste water. Different morphological properties were observed for these materials. Though, using the same acid concentration, SEM images of HCl hydrolyzed samples fibers did not showed the acid diffusion process and erosion of the fiber surface as did the SEM images of H3PO4 hydrolyzed MC fibers which showed the gradual acid diffusion process, eroded fiber surface and spindle-like individual crystals. The acid strength is implicated for the gradual diffusion and erosion of the fiber surface. HCl being a stronger acid than H3PO4 is able to quickly diffuse at a fast rate into the fiber. This process brings to our understanding of the fact that generating nanoparticles from biofibers does not depend only on acid concentration, temperature and time as earlier reported in many literatures, but also on acid strength according to the present work. This may be the reason H3PO4 is not commonly used for the preparation of nanoparticles from biofibers. Fiber metric image measurement for the MC nanoparticle showed the presence of nanofiber in range of 68 nm – 815 nm and these particles were the dominants as indicated by the fiber count histogram Figure A.11-A.12. A minor portion of the particles showed low intensity and ranged from 4.46 µm to several micrometers in dimension as reported by (Hong et al. (2012). Pore area measurement of fibers revealed the presence of most of the fibers with pore area which did not exceed 0.082 µm2 (82000 nm2). The above attributes

of the synthesized nanoparticles has endowed this particles the potential to be useful in removing pollutants in water due to their small size and high tendency to form hydrogen bonding network with metal ions and organic molecules thereby, trapping pollutants out of the feed system.

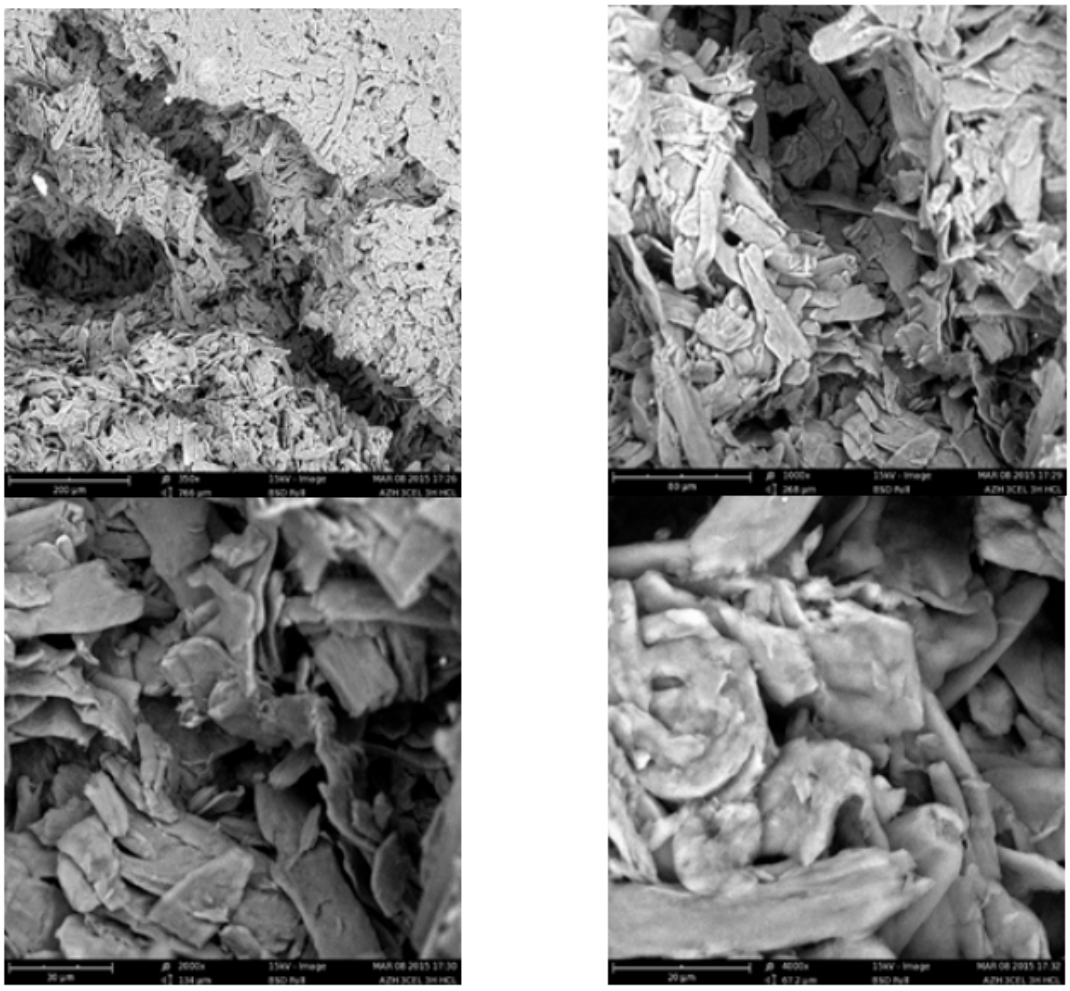

Fig. A.10: SEM Image of AZH3-CELL-3h-HCl

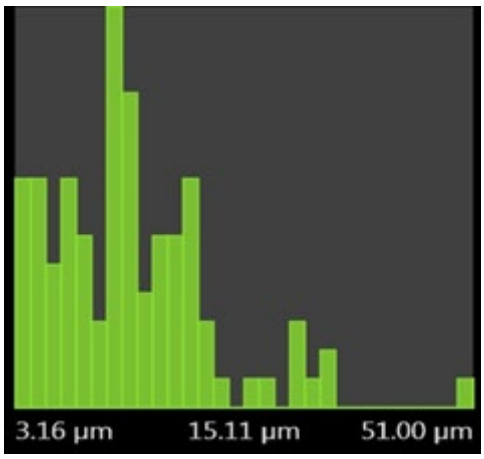

Fig. A.11: Fiber Length Histogram

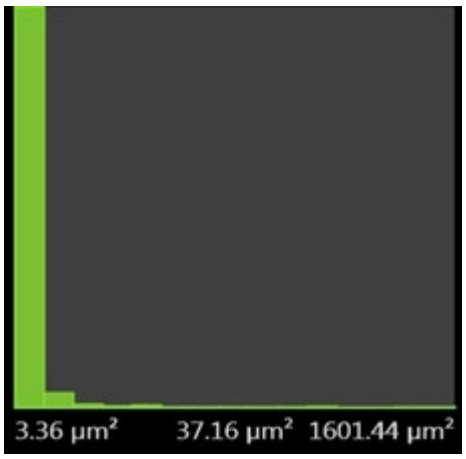

Fig. A.12: Fiber Pore Area Histogram

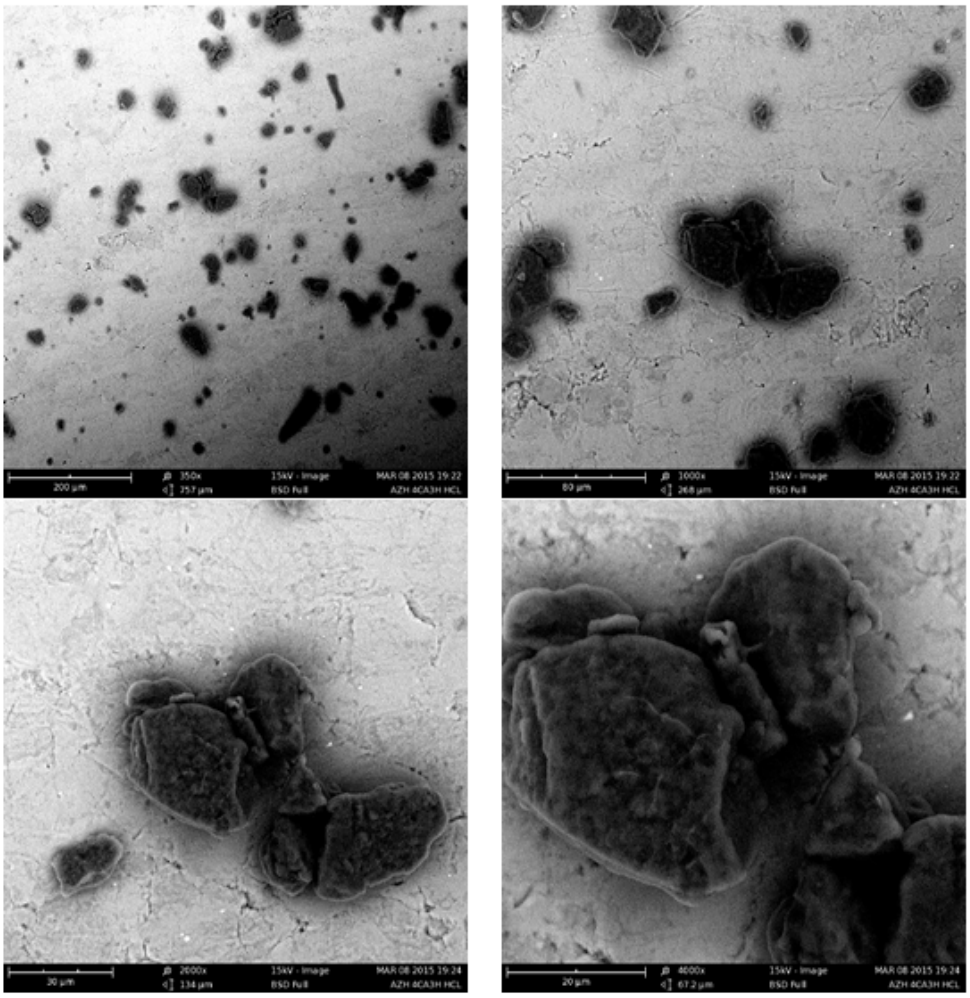

Fig. 16: SEM Image of AZH6-MC-3h-HCl

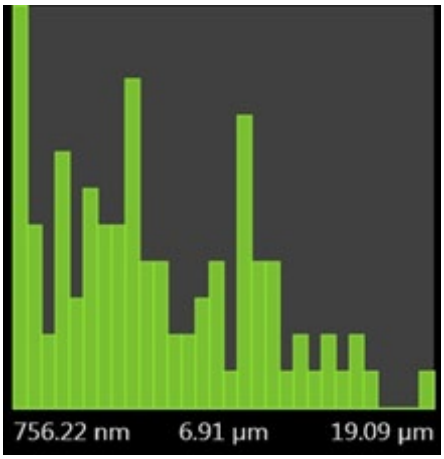

Fig. A.17: Fiber Length Histogram

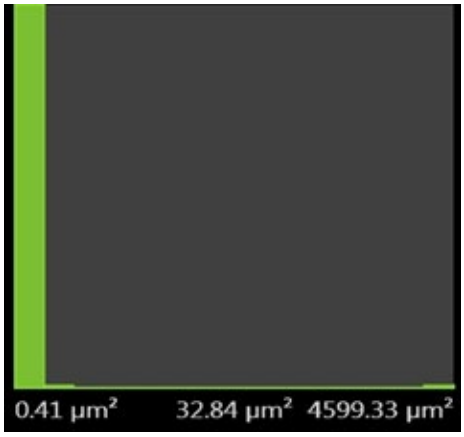

Fig. A.18: Fiber Pore Area Histogram

SEM Micrographs of 3/6h/H3PO4 hydrolyzed Samples:

The SEM images of synthesized cellulosic nanoparticles using H3PO4 are shown in Figures A.19-A.31. SEM micrographs of the samples hydrolyzed using H3PO4 revealed the presence different morphological characteristics of the hydrolyzed cellulose, CA and MC respectively. The presence of long cellulose acetate fibers in the hydrolyzed products was not observed in the SEM images of AZH11-CA-6h-H3PO4 and AZH8-CA-3h-H3PO4 shown in (Figs A.19 and A.22) unlike those reported by many authors (Polarz, Smarsly and Schattka, 2002; Joon-Pyo, Youn-Mook, Jae-Hak, Hyun-Shil, Phil-Hyun and Young-Chang 2007). The absence of elongated fiber micro bundles was evidenced by SEM images for AZH7-CELL-3h-H3PO4 and AZH10-CELL-6h-H3PO4 (Figures A.19 and A.25). The sample AZH8-CA-3h-H3PO4 nanoparticle crystals synthesized had different clusters of particle with interconnected web-like net-work as revealed by SEM images (Figure A.22) below, unlike sample AZH 7-CELL-3h-H3PO4 SEM images that showed a mixture of nano and short microcrystals (Figure A.19). At low and high magnification, crystalline particles appeared to be homogenously dispersed with well define interconnected structural network, large and small pore, inter-fibrillar network structures. These attributes were not found in AZH 7-CELL-3h-H3PO4 (Figure A.19). The fiber length distribution intensity (Figure A.23) clearly showed that high percentage of the fibers falls in range of 70 nm - 843 nm and agreed with other works on the nanocellulose crystals from different biomaterials using different acids under various reaction conditions (Denis et al. 2011; Susheel et al. 2011; Serge and Fernand (2013). The hydrolysis of MC with 64 % concentrated solution of H3PO4 for 1 h yielded a gel-like solution that was precipitated out of the solution when subjected to heat above its lower critical solution temperature (LCST), though, the gel was very unstable at temperature below its lower critical solution temperature. The stable gel was obtained from its solution by salting out. SEM images showed various sizes of inter-woven framework of single-like nanofiber having a homogenous phase of methylated cellulose nanoparticles with resemblances of bacteria colonies sample AZH12-MC-1h-H3PO4 (Figure A.28). The presence of different sizes and shapes of fragments of agglomerated individual block-like crystals with sharp corners were also seen for AZH10-CELL-6h-H3PO4 (Figure A.25) and there was complete absence of long fibers and bundles as compared to the 3 h of hydrolysis of both cellulose and CA. Nanocrystalline cellulose with various morphologies of this kind shown in this work has been reported. The SEM images of the 6 h hydrolysis showed clear evidences of the formation of cellulose acetate nanoparticle crystals with rod-like (Xiaoyun and Shuwen (2013) structures dispersed with homogenous phase (Amit (2013). Some clusters of these nano-rods were also observed (Figure A.31). At higher magnifications, both samples displayed surfaces that look rough and large with a compact agglomeration of nano-rods with a fibrillar interconnected web-like net-work for AZH10-CELL-6h-H3PO4. SEM images at higher magnification also revealed the porosity of the surface. Pores of various sizes and a close packing structure of interconnected network were observed at 350x and 1000x magnification for sample AZH11-MC-1h-H3PO4 (Figure A.28). At 1000x magnification, MC nanoparticles resemble those reported by (Amit 2013; Xiaoyun and Shuwen 2013). These particles also formed various sizes of agglomerates and aggregates attributed to the ability of hydrogels to form strong hydrogen bonding interactions. More so, the uniformity of the gel`s framework and their particle size is implicated for their tendency to form agglomerates through physical interaction (Zhong et al. 2011; Serge and Fernand (2013). The SEM image at 4000x magnification revealed further the interconnections between the individual nano-rod particles which have been attributed to their homogeneity, large surface area for contact, inter-chain and particle size (Figure A.28). SEM image of sample AZH10-CELL-6h-H3PO4 at 4000x showed the presence very tiny and fibrous entanglement of the nanofiber (Wen, Shenxue, Qisheng and Minzhu 2013). The web-like framework structure of AZH11-MC-1h-H3PO4 agreed with the reports in literature Wen et al. (2013) on crystalline particles and clustering due to agglomeration of tiny particles. This is due to surface charge exhibited as a result of H3PO4 treatment. The methylated cellulose nanoparticles had different morphologies from native methylcellulose micronized in acetone and DCM Ana et al. (2006). The porosity and surface area is due to the removal of amorphous cellulose regions and the strong intramolecular and intermolecular hydrogen bonding in network in nanocellulose crystals Anuj et al. (2014). The fiber length histogram intensity distribution obviously showed that high percentage of the fibers had length ranging from 72 nm to 874.33 nm for AZH10-CELL-6h-H3PO4 with very few of the fiber lengths intensity distribution in micro meter scale and these ranged from 5.06-18.07 µm (Figure A.26) and 90 nm - 1080 nm for AZH12-CA-6h-H3PO4 (Figure A.32), and 125 nm to 1500 nm for AZH11-MC-1H-H3PO4 (Figure A.29) which is in agreement with other reports (Denis et al. 2011; Zhong-Yan et al. 2011; Susheel et al. 2011; Serge and Fernand 2013; Anuj et al. 2014; Fernando 2010) with few of the fiber length measuring 4.11 µm – 14.33 µm. Fiber length of this type have been obtained using 44.1 mL /g and 64.8 % acid hydrolysis by Amit (2013). The pore area measurement of the fibers showed that a considerable number of fibers had pore area of 82000 nm2 (Figure A.27, A.29 and A.33). The pore area measurement of the fibers showed that most fibers had pore area of 82000 nm2 with virtually no fibers with pore area in range of 3.56 µm2 – 565 µm2 (Figure A.22 AZH8-CA-3h-H3PO4). The materials posses the potential for application as molecular sieves and where the properties are fit for use. Because of the uniform distribution of the pores coupled with above properties, MC nanoparticle can be used as molecular sieves in purification of both organic/inorganic polluted and waste water. It can also be used as matrix for the microencapsulation (host-guest relationship) for sustainable/controllable drug release. The homogenous nature of these particles will allow for the even distribution of pollutants in the crystal lattice of the material which will lead to the effective removal of pollutants from the feed solution. Films with homogenous phase can be prepared from this material due to the uniformity of the pores. The porous nature of the material provides information on the possibility of using it for

engulfing large organic and inorganic materials, atoms, ions and molecules that may be present in water/waste water not only on their surfaces, but throughout the bulk of the material by selective adsorption. CA is partially hydrophobic and hydrophilic, thus, it can absorb organic molecules from water as well as adsorption of water from organic solvent, it can acts as host molecules where they house organic guest molecules in their pores. For example, organic drugs for effective and control release for optimum performance and the adsorption of organic dyes.

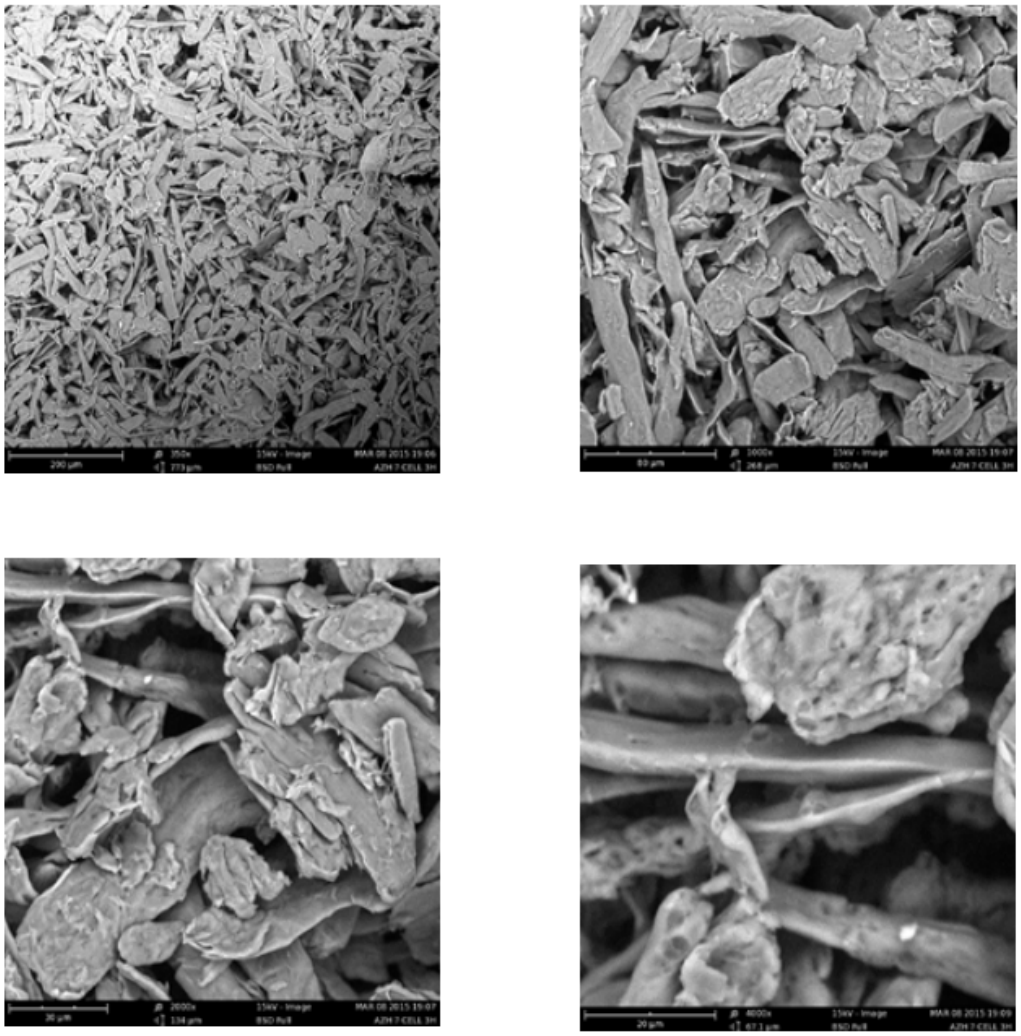

Fig. A.19: SEM Image of AZH 7-CELL-3h-H3PO4

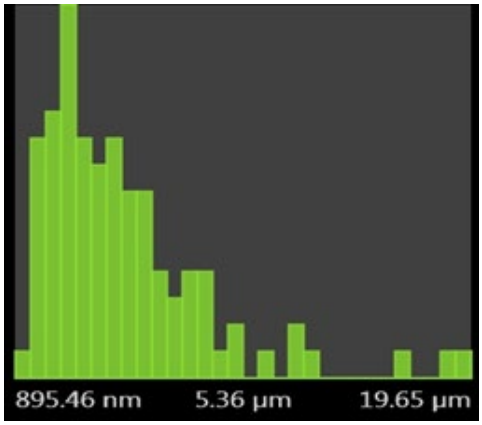

Fig. A.20: Fiber Length Histogram

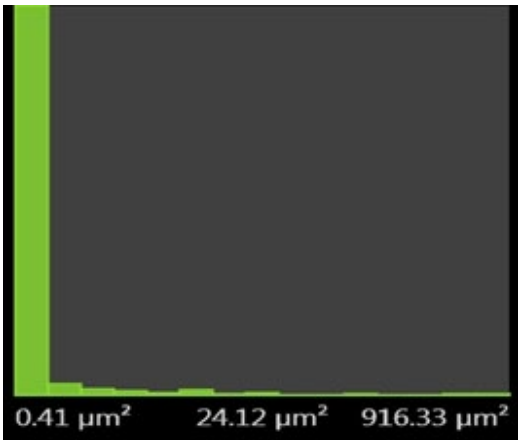

Fig. A.21: Fiber Pore Area Histogram

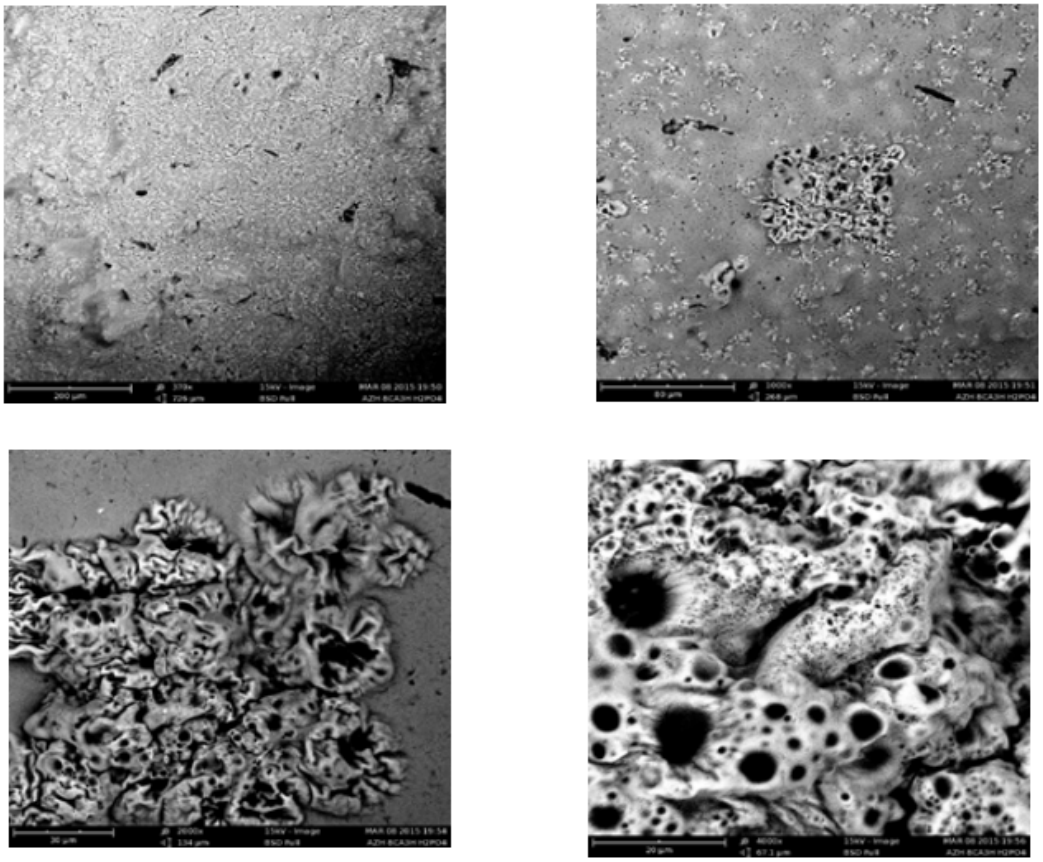

Fig. A.22: SEM Images of AZH8-CA-3h-H3PO4 Sample

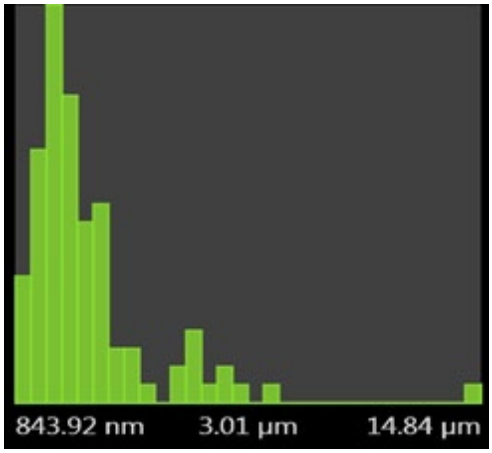

Fig. A.23: Fiber Length Histogram

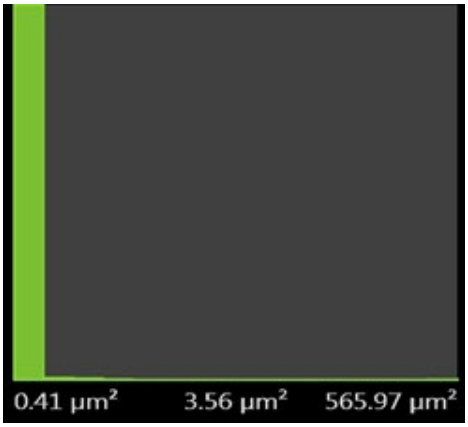

Fig. A.24: Fiber Pore Area Histogram

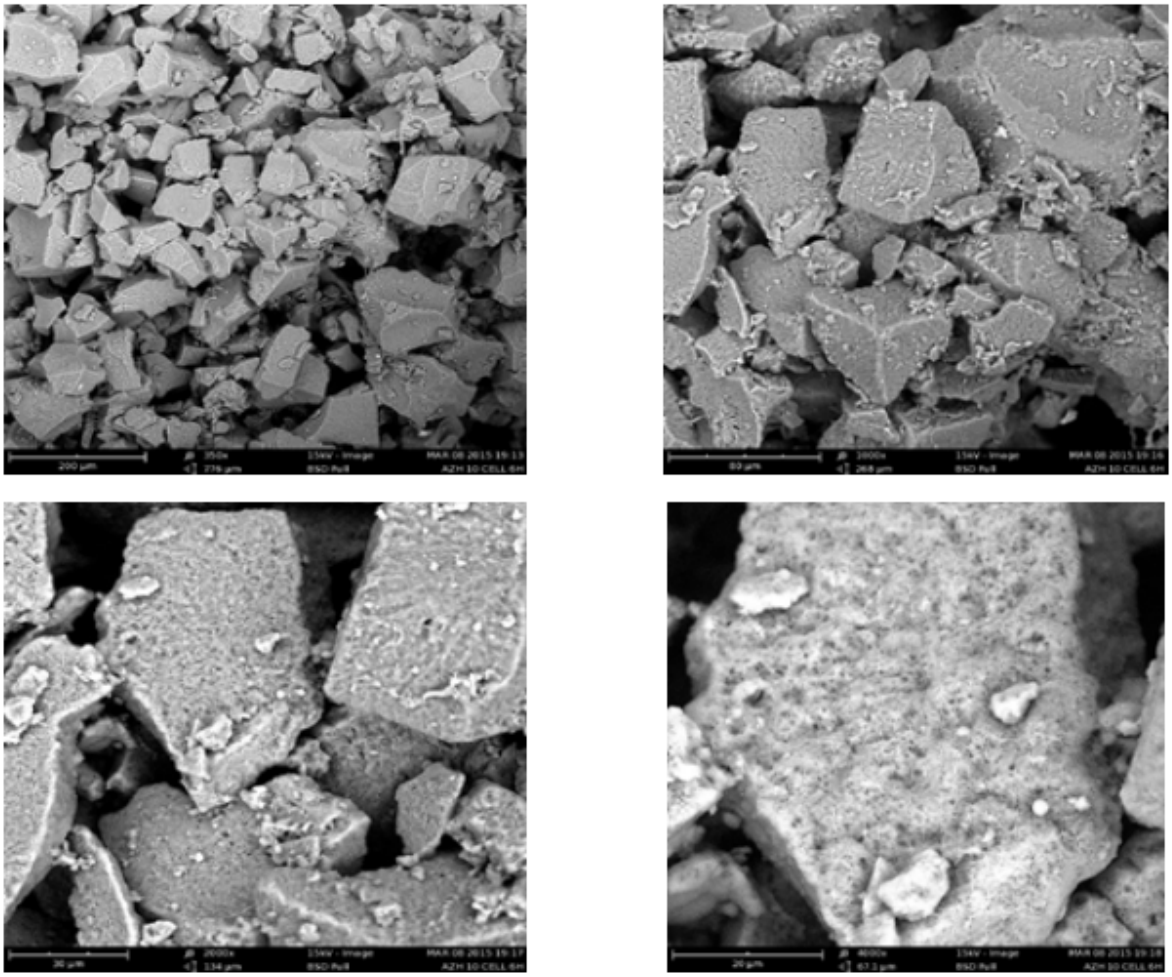

Fig. A.25: SEM Image of AZH 10-CELL-6h-H3PO4

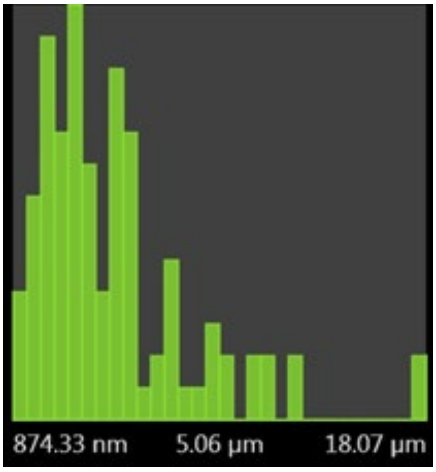

Fig. A.26: Fiber Length Histogram

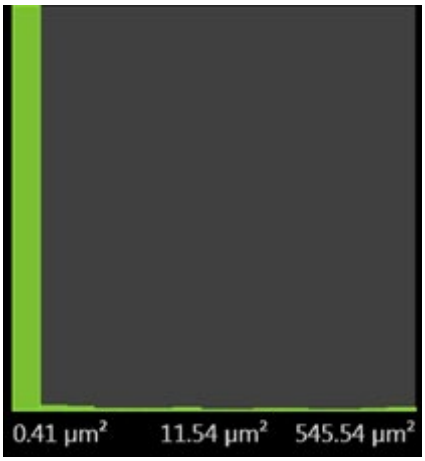

Fig. A.27: Fiber Pore Area Histogram

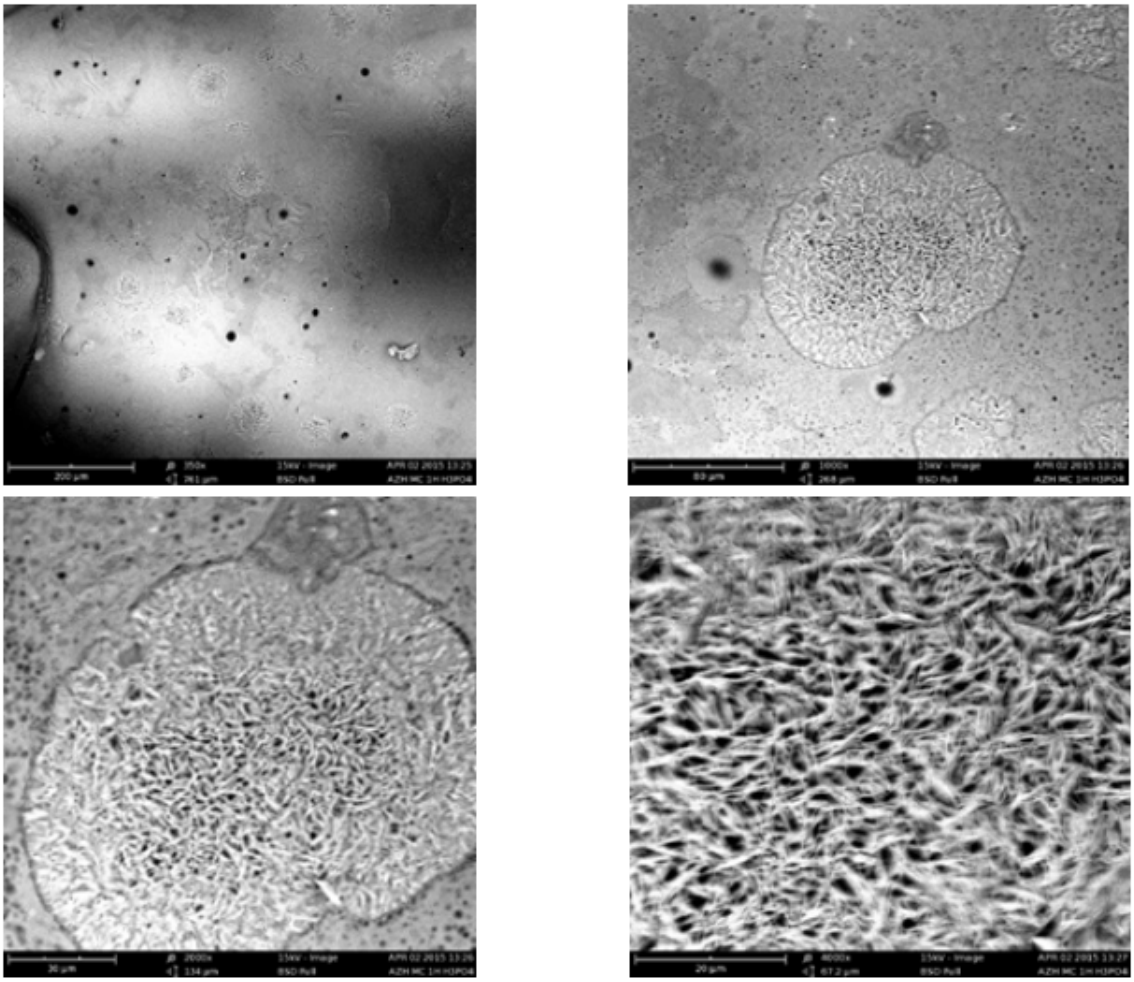

Fig. A.28: SEM Image of AZH11-MC-1h-H3PO4

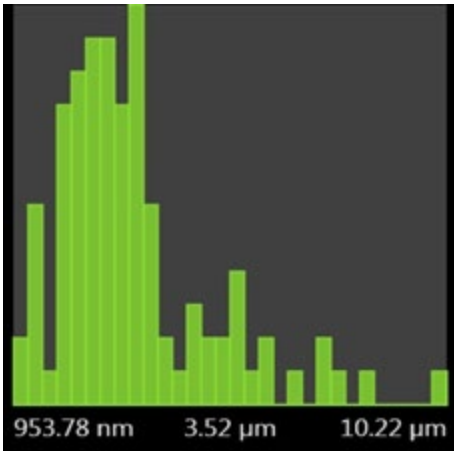

Fig. A.29: Fiber Length Histogram

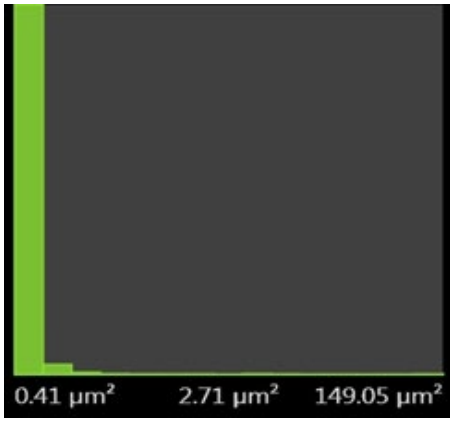

Fig. A.30: Fiber Pore Area Histogram

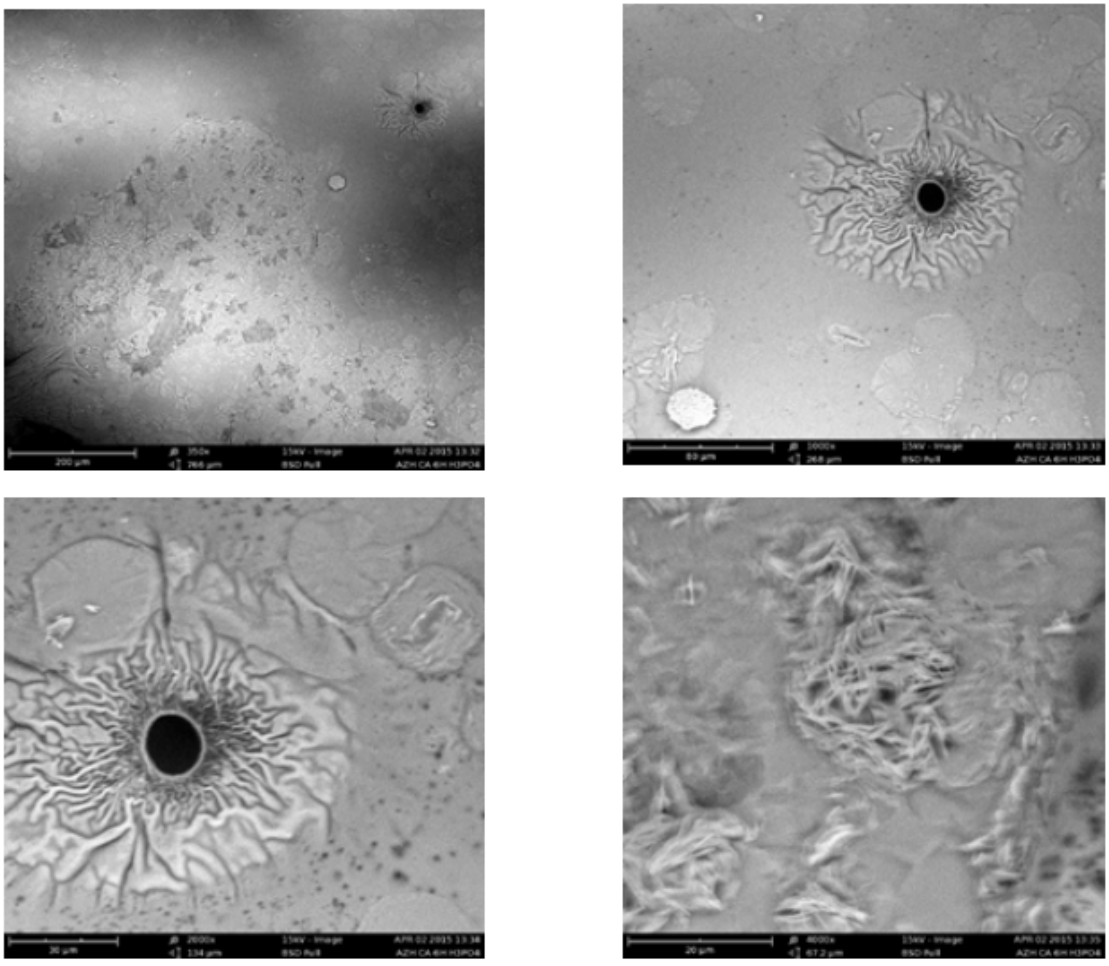

Fig. A.31: SEM Image of AZH12-CA-6h-H3PO4

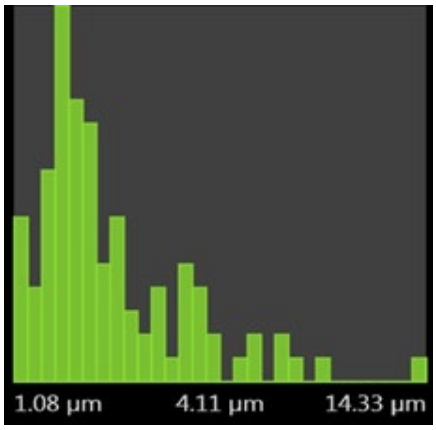

Fig. A.32: Fiber Length Histogram

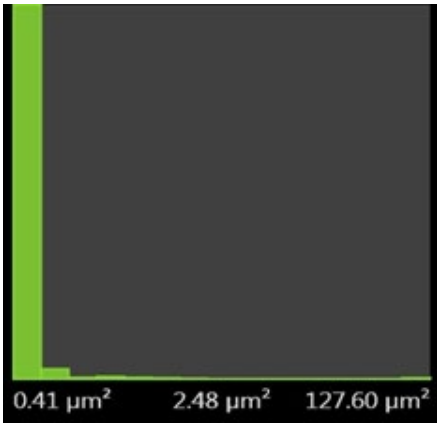

Fig. A.33: Fiber Pore Area Histogram

The effect of hydrolysis time on the particle size was observed for all samples synthesized and it depended on the material type, time, acid type, concentration and acid strength for the generation of nanoparticles. The SEM micrographs confirmed the nature of the nanoparticles synthesized with various types of morphology ranging from filamentous, spindle-like, aggregates/agglomerated, gel-like, needle-like and pores. The 6 h of hydrolysis for the CA using H3PO4 yielded nanoparticles that were observed to be very different from those obtained using HCl. The H3PO4 yielded rod-like individual crystalline particles that had homogenous phase with a close packing arrangement revealed at higher magnification. Though, not much work has been published on the use of H3PO4 acid for the preparation of nanocrystalline cellulose or its derivatives. The present work yielded similar results with that of the acids commonly use for the preparation of nanoparticles. The present work also showed that the strength of an acid is important for the generation of nanoparticles. BET surface area analysis of CELL-3h-H3PO4 and MC-3h-H3PO4 using N2 found CELL-3h-H3PO4, with 105.698 m2/g with micro pore volume, 0.01427 – 0.03676 cm3 and pore size (pore radius) of 1.510, 9.237, 1.730 nm, 1.324 nm while MC-3h-H3PO4 had 250.570 m2/g with micropore volume ranging from 0.03084 – 0.07939 cm3 and pore size, micropores and mesopores (pore radius) 3.266, 1.530, 9.237, 1.749, 1.324 nm were obtained and depended on the method employed for determination. Both single and multipoint BET surface data showed that the prepared nanoparticles had large surface area than those reported in literature for natural fibers and cellulose (Alexander, Ibon, Thomas Lampke, Bernhard, Artemis, Ilja and Hans-Heinrich (2002). The large surface area is attributed to small pore size of the nanoparticles prepared and was in agreement with literature report where 32 Å and 16 Å (3.2 nm and 1.6 nm) have been specifically mentioned to be the most common pore size for large surface areas of nanoparticles by Alexander (2002). The pore volumes of the nanoparticles obtained in this study are larger than those obtained by Albert (2005) through BET analysis of cellulose using N2 adsorption isotherms, but lower than the pore volumes obtained through water adsorption isotherms. Based on the recent applications and uses of membrane and depth filters for removal of bacteria and viruses from water and blood systems, it is important to stress that the prepared nanoparticles posses the potentials to be applied in this areas. Because of the small pore size of the particles compared to the sizes of these viruses; Severe acute respiratory syndrome (SARS) corona virus 80 – 120 nm in size, HIV virus, 100 – 120 nm in diameter, Avian flu, 80 - 120 nm in size, HBV 40 nm in size, mimivirus with 270 nm in diameter while some filoviruses having length up to 1400 nm with the capsid around 80 nm as described by (Zhao, Sugiyama, Miller and Miao (2008). Since membrane filtration is based on pore size of the membrane particles, thus particles larger than the pores will not be able to penetrate the pores and are thus separated.

Thermal Stability:

Thermal properties of cellulose and cellulosic materials have been intensively studied and well documented (Yucheng, Douglas, Yousoo, Alper, Zhiyong and Mandla (2013). Cellulose as one of the major components of cellulosic material has systematic thermal decomposition pattern that is principally responsible for the production of flammable volatiles, which are released through dehydration, hydrolysis, oxidation, decarboxylation and transglycosylation processes (Yuncheng et al. (2013). The pathway of thermal decomposition and the composition of the cellulose fibers (residual hemicelluloses) are influenced by many physical and chemical factors such as temperature, ambient environment, size and texture of the cellulose sample, crystallinity, presence of impurities such as metals, and other parameters (Yuncheng et al. (2013). Thermal characteristics of the cellulosic nanoparticles in this study were considered at T95, T90 and Tmax. The T95, T90 and Tmax of the prepared nanoparticles varied significantly. For the azeh2, azeh4 and azeh11, T95 for the mass loss of 5 wt % occurred at 332.39 oC, 320.60 oC and 297.51 oC with T90 for a 10 wt % mass loss at 348.92 oC, 345 oC and 315 oC. At

this temperature, depolymerisation of anhydrocellulose began to yield volatile compounds like CO, CO2 and H2O. At Tmax the decomposition of the nanomaterials were attained for the samples, azeh2, azeh4 and azeh11 at 405, 401 and 375 oC respectively. It can be seen that from the on-set decomposition temperature at T95 and T90, the decomposition of the nanomaterials persisted up-to 680 oC. The temperature above this region leads to decomposition of levoglucosan which gives rise to a variety of low molecular weight fission products, including hydrocarbons and hydrogen as well as CO, CO2 and H2O Yucheng et al. (2013). The maximum wt loss rate for these samples was reached at 405, 401 and 375 oC and the nanocellulose/propylated nanoparticle was completely pyrolyzed at 900 oC. The samples, azeh2 and azeh4 showed similarities in their decomposition pattern which is attributed to the re-organization of crystal lattice of the cellulose nanoparticles (Yiying (2013). The TGA of azeh2, azeh4 and azeh11, indicated that the nanoparticles showed almost the same TGA curve trend. Sample azeh11, was less thermally stable due to the propyl substituent in the structure. Azeh8, azeh10, azeh12 and azeh18 displayed similarities in their decomposition pattern. At T95, 5 wt % loss of the nanomaterial was attained at 389.37, 287.45, 452.14 and 411.09 oC. But an extended decomposition temperature for the samples was observed at T90 at 416.22, 351.89, 487.36 and 5 08.55 oC. The Tmax for these samples were 430, 430 and 525 oC and were higher compared to other samples. These materials showed an extended decomposition over the whole temperature range, starting well below 300 oC and persisted above 900 oC. At 900 oC the remaining solid nanomaterials was about 50 wt %. The wide temperature decomposition range has been attributed to the different activities of the chemical bonds present on its structure Juan, Vera, Viviana and Analia (2008). The DTG peak of azeh10 showed a small broad peak which appeared during the decomposition of the sample at 370 oC on the left close to the main peak at 420 oC, attributed to the breakdown of hemicelluloses Juan et al. (2008). The small broad peak which appeared slightly above 150 oC is due to the decomposition of the substituent acetyl group. The decomposition of azeh8, azeh10, azeh12 and azeh18 was slower compared to the decomposition of other nanomaterials and it extended over 900 oC temperature range with about 50 wt % of the materials left. With the extended thermal stability of these materials at T90, the stability is due to their crystalline order and size distribution of the nanomaterials Yucheng et al. (2013).

The DTG peak of the nanoparticles occurred well at 405 °C for azeh2, 401 oC for azeh4, 375 oC for azeh11, 430 oC for azeh8 and azeh10 and 525 oC for azeh12, as shown in appendix H. This result suggests that celluloses with higher TCI, LOI and hydrogen bond index (HBI) have higher thermal stability probably due to the much more hydrogen bonds between cellulose chains that can result in more ordered and packing cellulose regions, this in turn possibly increasing the thermal decomposition temperature of cellulose Matheus et al. (2012).

The TGA-DTG data of the studied nanomaterials showed that the thermal stability of the nanomaterials was improved as shown by the increase in the value of initial decomposition temperature at T95 and T90 respectively. The on-set temperature (To) for the bulk CA and native cellulose have been reported at 250 oC, for CA and 216 oC for native cellulose Abir and Azza, 2014; Yucheng et al. 2013). The TGA-DTG of the nanomaterials indicated extra thermal stability compared to their bulk counterpart.

Ft-Ir Analysis:

FTIR spectra of nanocellulose particles obtained from Cellulose, MC, CA using HCl, H2SO4 and H3PO4 as shown in Figure I - VII. Table 1 shows the band positions and the corresponding functional groups in samples.

Band position (cm^{-1})	Band Assignment (Functional group)	References
3931-3445 and 3379-3343	-OH of O(2)H-O(6) and O(3)H-O(5) intramolecular hydrogen bonding.	(Zuezhu, Fei, Long, Zhu, Darrin, and Dennis 2013; Li 2012).
3361-3176	-OH of O(6)H-O(3) is due to intermolecular hydrogen bonding.	(Xu et al. 2011; Matheus, Heitor and Zattera 2014; Mayra et al. 2015).
2726-2969	C-H stretching vibration of aliphatic CH_2 in cellulose and symmetry and asymmetry stretching vibrations in CNCs.	(Youssef, Henri and Michel 2006; Xiaolin, Shengrui, Maofa, Lingyan, Junchao, Changyan and Weiguo 2012).
1791-1715	C=O of the ester of acetyl group and carboxylic acid groups in cellulose.	(Chih-Ping et al. 2010; Hassan, Ilari, Sarah, Dermot and Dimitris 2011; Li 2012; Vigneshwaran and Prasad 2011)
1652-1633	Assigned to O-H characteristic bending vibrations of bound water.	(Lani, Ngadi, Johari and Jusoh 2014; Nor, Salma and Ishak 2014).
1557-1505	May have arisen due to residual hemicelluloses at the amorphous region.	(Adapa, Karunakaran, Tabil and Schoenau 2009; Francesca, Roberta, Donato, Giuseppe and Alfonso 2012).
1425-1420	CH_2 bending mode for both cellulose crystals I and amorphous cellulose.	(Chih-Peng et al. 2009; Anuj et al. 2014).
1430 and 897	CH_2 deformation vibrations and C-O-C glycosidic linkages in CNCs synthesized (unique fingerprint to crystalline cellulose I.	(Vigneshwaran and Prasda 2011; Yiyin, 2011; Mizi, Dasong and Biao 2012; Li 2012; Teboho 2012; Nor et al. 2014; Anuj et al. 2014; Mayra et al. 2015).

Band position (cm^{-1})	Band Assignment (Functional group)	References
1377-1312	C-H in-plane symmetrical deformation vibrations of many types of CH and CH_2 in -C-CH_3 of the acetate group.	(Vigneshwaran and Prasda 2011; Mizi, Dasong and Biao 2012; Yiyin 2011; Teboho 2012; Li 2012; Anuj et al. 2014; Nor et al. 2014; Mayra et al. 2015).
1335	C-H bending mode in cellulose and appeared to have shifted to higher absorption bands for all samples.	(Francesca et al. 2012; Teboho 2012; Anuj et al. 2014; Nor et al. 2014; Mayra et al. 2015).
1312, 1316 and 1302	CH_2 weak wagging vibrations of C6 in crystallized cellulose I observed at lower absorption bands due to the amount of crystalline form of cellulose in samples.	(Vigneshwaran and Prasda 2011; Yiyin 2011; Mizi, Dasong and Biao 2012; Li 2012; Teboho 2012; Nor et al. 2014; Anuj et al. 2014; Mayra et al. 2015).
1203	C-O is due to weak deformation in acetate and -OPO_3- (P=O) absorption	(Adapa 2009; Yiyin 2011; Xu et al. 2011; Nor et al. 2014; Teboho 2012; Yussuf et al. 2006; Xuezhu et al. 2013; Chih-Peng et al. 2010; Li 2012; Anuj et al. 2014; Mayra et al. 2015)
1060 and 1184-1112	C-O and C-O-C stretching vibration of β-glycosidic linkages of the ether group in CNCs.	(Francesca, *et al*., 2012; Teboho, 2012; Anuj *et al*., 2014; Nor *et al*., 2014; Mayra *et al*., 2015. Yiyin, 2011).
900-1003	P-O, P-O-C and P-OH shoulder vibration	(Granja et al., 2001; Vanja et al., 2015)

Band position (cm^{-1})	Band Assignment (Functional group)	References
1166, 1164, 1162, 1060, 1058	Assigned to C-O and C-O-C stretching vibrations of glycosidic linkages specific to cellulose I (CNCs).	(Adapa 2009; Yiyin 2011; Xu et al. 2011; Nor et al. 2014; Teboho 2012; Yussuf et al. 2006; Xuezhu et al. 2013; Chih-Peng et al. 2010; Li 2012; Anuj et al. 2014; Mayra et al. 2015).
1058	C-O stretching at C3 position.	(Teboho 2012; Anuj et al. 2014; Yussuf et al. 2014).
1156	Assigned to C-O stretching in amorphous cellulose was missing in all the CNCs samples.	(Chih-Peng *et al*. 2010; Vigneshwaran *et al*. 2011; Yiyin 2011; Xu et al. 2011; Xiaolin et al. 2012; Meiling et al. 2013; Nor et al. 2014; Mayra et al. 2015).
990	Is connected to C-O stretching vibrations at the crystallite region of cellulose.	(Adapa et al. 2009; Hassan et al. 2011; Francesca et al. 2012; Nor et al. 2014).
896-846	CCO and C-C-H deformation modes at C5 and C6 positions and C-O-C and C-O-H due to anomeric carbon stretching vibrations of β-glycosidic linkages between glucose units in CNCs.	(Yussuf et al. 2006; Xu et al. 2010; Vigneshwaran et al. 2011; Teboho 2012).
893	C-O is a characteristic absorption in cellulose I.	(Chih-Peng et al. 2010; Vigneshwaran et al. 2011; Xu *et al*., 2011; Yiyin, 2011; Xiaolin et al. 2012; Meiling et al. 2013; Nor et al. 2014; Mayra et al. 2015).
699-616	Related to C-O-H out-of-plane wagging and twisting modes in AGU.	Xu et al. 2010; Teboho 2012).
560-405	Characteristic bands corresponding to CNCs skeletal vibrations.	Xu et al. 2010; Teboho 2012).

Generally, the nanocellulose isolated EC, MC, CELL, and CA showed the basic structural features of cellulose I profile denoted by intramolecular hydrogen bonding between various types of –OH groups in cellulose materials ranging from 3931-3171 cm-1 (Carmen-Mihaela, Maria-Cristina, Ghita, Cornelia, Dimitris and Stefan 2007; Chih-Ping, I-Chen, Kuo-Jung and Yuan-Shing 2010; Xu and Wei-Dong 2010; Dan 2011; Diana, Florin and Valentin 2011; Vigneshwaran and Prasad 2011; Yakubu, Tanko and Sani 2011; Li 2012; Maria, Arja-Helena, Youssef, Leena-Sisko, Joel, Alexander and Orlando 2013; Meiling, Shujun, Mingxin, Chunjie, Feng and Wei 2013; Mayra, Lucimara, Nelson and Ljubica 2015). These absorptions depend on their positions on the surface of cellulose crystals. The absorption peaks at 3931-3445 cm-1 and 3379-3343 cm-1 have been assigned to O(2)H-O(6) and O(3) H-O(5) intramolecular hydrogen bonding while 3361-3176 cm-1 is due to intermolecular hydrogen bonding between O(6)H-O(3) in cellulose materials (Li 2012; Zuezhu, Fei, Long, Zhu, Darrin and Dennis 2013). The absorption peak that occurred near 4000 cm-1 in samples are attributed to more of –OH groups on the CNCs particle surface and subsequent formation of intramolecular hydrogen bonding. Another important reason that may have led to high absorbance peaks in CNCs samples, is the tendency of C-O-C in CNCs to accept a proton (H+) from –OH donor groups to form intermolecular hydrogen bonding (Xuezhu et al. (2013). The band at 2726-2969 cm-1 is due to C-H stretching vibration of aliphatic CH2 in cellulose (Xu et al. 2011; Matheus, Heitor and Zattera 2014; Mayra et al. 2015). The band at 2726 cm-1 is specific to C-H (methylene) stretching vibrations while the peak absorption at 2969-2953 cm-1 was prominent and has been assigned to C-H (methylene) symmetry and asymmetry stretching vibrations in CNCs (Xu et al. 2011; Matheus, Heitor and Zattera 2014). It was observed that this peak became flattened and broadened for all the nanocellulose products where it appeared and is due to collapse of cellulose at the amorphous region and increased crystallinity of CNCs.

The peak which occurred at 1791-1715 cm-1 accounts for the absorption due to CO of the ester of acetyl group and carboxylic acid groups in cellulose (Youssef, Henri and Michel 2006; Xiaolin, Shengrui, Maofa, Lingyan, Junchao, Changyan and Weiguo 2012). The absorption owing to the CO of carboxylic acid groups may be due to oxidation of some of the accessible –OH groups forming uronic acids of hemicelluloses.

The absorbance peaks at 1652-1633 cm-1 is assigned to O-H characteristic bending vibrations of bound water and could have originated from the adsorption of atmospheric vapour and water molecules during storage onto cellulose nanocrystals (Chih-Ping et al. 2010; Xu et al. 2010; Hassan, Ilari, Sarah, Dermot and Dimitris 2011; Vigneshwaran and Prasad 2011; Li 2012; Teboho 2012; Meiling et al. 2013). The absorption band at 1557-1505 cm-1, found virtually in almost all the samples, may have arisen due to residual hemicelluloses at the amorphous region (Lani, Ngadi, Johari and Jusoh 2014; Nor, Salma and Ishak 2014). The presence of these peaks may be due to the fact that the samples were not dialyzed against distilled water in order to remove other soluble materials that escape during the centrifugation of the samples. The band at 1425-1420 cm-1, usually for both cellulose crystals I and amorphous cellulose assigned to CH2 bending mode (Adapa, Karunakaran, Tabil and Schoenau 2009; Francesca, Roberta, Donato, Giuseppe and Alfonso 2012). The spectral bands at 1430 and 897 cm-1 have been reported to be a unique fingerprint to crystalline cellulose I Chih-Peng et al. (2009). A shift in these bands was observed at 1488-1455 cm-1 and 997-891 cm-1 assigned to CH2 deformation vibrations and C-O-C glycosidic linkages in CNCs synthesized, is a pointer to increased CNCs contents in samples (Chih-Peng et al. 2009; Anuj et al. 2014). This confirms the structural morphology of CNCs was intact, and the increased of the bands intensity was due to increase in cellulose crystallinity Diana et al. (2011). The cellulose acetate (CA) sample gave this important band at 1377-1312 cm-1, and has been attributed to CH symmetrical deformation vibration in -C-CH3 of the acetate group. All other cellulose samples showed this band in the range 1377-1312 cm-1, owing to in-plane CH symmetrical deformation vibrations of many types of CH and CH2 which may be due to partial removal of hemicelluloses in the dislocation (amorphous) regions of cellulose chain during acid hydrolysis (Yiying 2011; Vigneshwaran and Prasda 2011; Mizi, Dasong and Biao 2012; Li 2012; Teboho 2012; Anuj et al. 2014; Nor et al. 2014; Mayra et al. 2015). The peak observed at 1335 cm-1 is assigned to C-H bending mode in cellulose and has shifted to higher absorption bands at 1375 cm-1 in AZH7/CELL/H3PO4, 1376 cm-1 in AZH10/CELL/H3PO4, 1377 cm-1 in AZH3/CELL/HCl, 1376 cm-1 in AZH8/CA/H3PO4 and were also found at lower absorption bands at 1312 cm-1, 1316 cm-1 and 1302 cm-1 due to the amount of crystalline form of cellulose in these samples. The band peaks at 1377-1375 cm-1 of the CNCs samples had strong valleys that were almost similar in all samples and corresponded to cellulose with high crystallinity index. The bands at 1302 cm-1, 1312 cm-1 and 1316 cm-1 are usually due to CH2 wagging vibrations of C6 in crystallized cellulose I were weak in accordance to literature reports (Francesca et al. 2012; Teboho 2012; Anuj et al. 2014; Nor et al. 2014; Mayra et al. 2015). These are pointers to increased crystallinity of CNCs samples while content of amorphous cellulose is negligible. The band at 1370 cm-1 is an important characteristic band for structural carbohydrates. This band increased in CA samples and appeared at 1377 cm-1 and 1376 cm-1 used to identify C-H bending deformation of -C-CH3 in acetate group in crystalline cellulose. A shift in this band is due to removal of amorphous cellulose in the cellulose chain. An important band at 1203 cm-1 occurred which is due to C-O weak deformation in acetate and C-O-P of -OPO3- absorption Yiying (2011). Bands typical to cellulose materials were found in almost all the nanocellulose samples at 1060-1003 cm-1 and 1184-1112 cm-1 assigned to C-O, C-O-C stretching vibration of β-glycosidic linkages of the ether group in CNCs (Yussuf et al. 2006; Adapa 2009; Chih-Peng et al. 2010; Xu et al. 2011; Yiying 2011; Li 2012; Teboho 2012; Xuezhu et al. 2013; Anuj et al. 2014; Nor et al. 2014;

Mayra et al. 2015). But there are specific bands that confirmed the structural morphology of CNCs in the samples and these are 1166 cm-1, 1164 cm-1, 1162 cm-1, 1060 cm-1, 1058 cm-1 assigned to C-O and C-O-C stretching vibration of glycosidic linkages in cellulose I Teboho (2012). 1058 cm-1, is a unique band peak for C-O stretching at C3 position Li (2012). These bands gave a clear evidence of the intact structural morphology of CNCs after acid hydrolysis. The band at 1156 cm-1 assigned to C-O stretching in amorphous cellulose was missing in all the CNCs samples owing to a shift in the absorption peak of this band to 1184 cm-1, 1166 cm-1 and 1164 cm-1 and 1158 cm-1 due to increased crystallinity of samples (Adapa et al. 2009; Francesca et al. 2012; Hassan et al. 2011; Nor et al. 2014). This was a clear evidence of the amount of crystalline cellulose in samples. Other bands that further gave evidence of the intact structural morphology of CNCs are sharp bands found in the region 896-846 cm-1, in all CNCs samples. The absorptions have been assigned to, CCO, C-C-H deformation modes at C5 and C6 positions and C-O-C and C-O–H of the anomeric carbon stretching vibrations of β-glycosidic linkages between glucose units and are all characteristics bands in cellulose, implying that the morphology of CNCs was not destroyed by acids (Chih-Peng et al. 2010; Vigneshwaran et al. 2011; Xu et al. 2011; Yiyin 2011; Xiaolin et al. 2012; Meiling et al. 2013; Nor et al. 2014; Mayra et al. 2015). These bands appeared as very sharp valleys, indicating the crystallinity of the samples. The band at 893 cm-1 is characteristic absorption of the C-O in cellulose I and other β-glucosans with β-linked bonds. A new band appeared in all CNCs products at 722 cm-1, sharp and similar in all CNCs samples. This peak is assigned to –OH- in-plane vibration in CNCs. The band at 990 cm-1 is connected to C-O stretching vibrations at the crystallite region of cellulose. These bands are characteristic band in cellulose, indicating that the structure of CNCs was not affected (Yussuf et al. 2006; Anuj et al. 2014). The absorbance peak at 699-616 cm-1 is related to C-O-H out-of-plane wagging and twisting modes in AGU (Yussuf et al. 2006; Vigneshwaran et al. 2011; Teboho 2012).

The absorption band at 1791-1715 cm-1 is due to carbonyl (CO) stretching vibrations. The CA sample showed this band at 1790, 1738 and 1715 cm-1 respectively. The increase in the band intensity at 1790 cm-1 has been attributed to the oxidative degradation of cellulose due to heating/atmospheric oxygen. This band was missing in AZH11-CA-6h-H3PO4 , and is due to deacetylation, owing to excessive oxidation and removal of acetyl groups due to the impact of the reaction time in line with literature reports (Francesca et al. 2012; Hassan et al. 2011; Zheng 2013). This band was also observed in cellulose samples and has been attributed to the oxidation of cellulose giving rise to γ-lactones, carboxylic acids and dialdehyde and ketones (Francesca et al. 2012). The reason may have been the reaction temperature, moisture and continuous contact with water molecules during storage of the suspension in aqueous medium Juergen, Steven, Wilson and Dirk (2011).

The band absorption at 669–616 cm-1 is due to C-O-H out-of-plane bending vibration which is characteristic of cellulose materials. Other characteristic bands corresponding to CNCs skeletal vibrations occurred at 560-405 cm-1 (Xu et al. 2010).

Crystallinity Analysis:

XRD pattern for all samples at different treatment conditions are shown in Appendix A-G. XRD analyses of the samples were done in order to determine the changes of the crystallinity and amorphous region of the acid hydrolyzed cellulose, CA and MC respectively. Crystallinity index is the ratio of the diffraction from a crystalline region to the total diffraction of sample Nor et al. (2014). The value of crystallinity index (CI) was calculated using empirical Segal equation (Pereira, Herman, Maria, Daniella, Sandra and Maria 2011; Saxena 2013; Lani et al. 2014). All H3PO4-MC nanoparticle and H3PO4-CA nanoparticle obtained under the 1, 3 and 6 h hydrolysis showed a unique sharp peak at (2theta = 6.1o, 10o, 22.3o) representing the crystalline area in MC and CA. The peak at (2theta = 18.1 in these samples was broad and thus, emanated from the amorphous regions and the randomly distributed acetyl and methyl groups which are difficult to re-orient themselves into a close packing and regular order again. For this reason, cellulose acetate is known to be a semicrystalline polymer Abdel-Naby and Ghamdi (2014) and a decrease in crystallinity is observed Loo, Hashim and Leh (2012). These samples had the lowest CI index value of (25 %) attributed to the presence of high amount of amorphous regions and short reaction duration employed for their synthesis. Another reason may be due to the formation of nano-hydrogel, very liable to absorbing water molecules during storage and may have resulted to decrystallisation of these samples. Another important reason for the low crystallinity index value for MC and CA may be attributed to substituent groups (methyl, in MC and acetyl, in CA) being organic and their contribution to hydrophobicity of the samples. Methyl groups have been implicated for the low crystallinity of substituted polyesters Albert, Leen, Adriaan, and Ivan (1995). Other samples showed peak intensities around 15.1o, 17.5o, 22.3o, and 34.3 o at 2Theta for the (101), (101), (002) and (040) planes, respectively, and they can be identified as the CNCs diffraction peaks while the observed peaks at 12.5o, 20.1o and 34.3o in almost all the samples can be attributed to co-existence of both CNCs (Cellulose I) and the amorphous (Cellulose II) cellulose particles (Pereira et al. 2011; Xuezhu et al. 2013; Nor et al. 2014). The CI value of other samples was a clear indication of the high amount of CNCs in the samples, and the highest calculated was 80 % for the sample with AZH3-CELL-3 h-HCl. This is due to the nature of the acid used; as this was not obtained in samples treated using H3PO4, and may be due to its low viscosity and strength, which may affect its diffusion into the cellulose structure. Other cellulose nanocrystals (CNCs) had 53, 63, 65, 68 percentage value of CI as reported in some literatures (Xuezhu et al. 2011; Anuj et al. 2014). It was observed that increase in CI was influence by time, and acid strength as shown by the 3 h and 6 h hydrolysis as documented in some literatures (Filponen 2011; Narjes, Omid and Hossein 2012). In this work, samples were stored as suspension, and the long time storage of the samples under aqueous medium could have affected

the CI values due to absorption of water molecules and subsequent re-organization of the hydrogen networks in CNCs.

References:

1.Anna, K., Maria, H., Yulia, L., Anatoliy, K., Anatoliy, P., Tatiana, M., 2012. Oxo-biodegradability of polyethylene blends with starch, cellulose and synthetic additives. chemistry & chemical technology, 6, (4), 405-413.

2.Atanu B., Badal C. Saha, John W. Lawton, Shogren R. L., Willett J. L., 2006. Process for obtaining cellulose acetate from agricultural by-products. Carbohydrate Polymers, 64, 134-137.

3.Azeh, Y., Tanko, M. U., Sani, S. D. M., 2011. Chemical Modification of Microcrystalline Cellulose: Improvement of Barrier Surface Properties to enhance Surface Interactions with some synthetic polymers for Biodegradable Packaging Material Processing and Applications in Textile, Food and Pharmaceutical Industry. Advances in Applied Science Research, 2 (6), 532-540.

4.Ana Filipa de Assunçao Xavier: A Study on the Homogeneous and Surface Initiated Atom Transfer Radical Polymerization of Thermo-responsive Polymers from Regioselectively and Non-Regioselectively Substituted Cellulose Derivatives. A Thesis Submitted in Partial Fulfillment of the Requirements For the Degree of Doctor of Philosophy in the Faculty of Graduate and Postdoctoral Studies (Forestry). The University of British Columbia (Vancouver) February, 2014.

5.Anuj, K, Yuvraj, S. N, Veena, C., Nishi, K. B., 2014. Characterization of cellulose nanocrystals produced by acid-hydrolysis from sugarcane bagasse as agro-waste. Journal of Materials Physics and Chemistry, 2(1), 1-8.

6.Adapa, P., Karunakaran, C., Tabil, L., Schoenau, G., 2009. Potential applications of infrared and raman spectromicroscopy for agricultural biomass. Agricultural Engineering International: the CIGR Ejournal. Manuscript 1081, 11, 2009.

7.Albert, J. B. L., Leen, V. D. D., Adriaan, B., Ivan, V., 1995. Effect of methyl groups on the thermal properties of polyesters from methyl substituted 1,4-butanediols and 4,4'-biphenyldicarboxylic acid. Journal of Polymer Science: Part A Polymer Chemistry, 33,493-504.; John Wiley & Sons, Inc. CCC O & t7-624X/95/030493-12.

8.Abdel-Naby, A. S., Azza, A. A., 2014. Chemical modification of cellulose acetate by diallylamine. Int.J.Curr.Microbiol.App.Sci., 3(6): 10-24; ISSN: 2319-7706.

9.Alexander, B., Ibon, A. A., Jurgen, S., Thomas, L., Bernhard, W., Artemis, S., Ilja, S. Hans-Heinrich, L., 2002. Surface characterization of flax, hemp and cellulose Fibers: Surface properties and the water uptake behavior. Polymer Composites, 23 (5), 872-894.

10.Batista, A, Ferreira, I. and Borges, J. 2013. Cellulose-Based Bioelectronic Devices.

11.Cellulose–Medical, Pharmaceutical and Electronic Applications. 68-82.

12.http://dx.doi.org/10.5772/56721.

13.Carmen-Mihaela, P., Maria-Cristina, P., Ghita, S., Cornelia, V., Dimitris, S. A., Stefan, W., 2007. Spectral characterization of eucalyptus wood. Applied Spectroscopy, 61 (11), 2007.

14.Chih-Ping, C., I-Chen, W., Kuo-Jung, H., Yuan-Shing, P., 2010. Preparation and characterization of nanocrystalline cellulose by acid hydrolysis of cotton linter. Taiwan J. for Sci., 25 (3), 251-64.

15.Dieter, K., Hans, P. Schmauder, Thomas, H. Cellulose. Institute of Organic and Macromolecular Chemistry, Friedrich Schiller University of Jena, Humboldtstrasse 10, D-07743 Jena, Germany.

16.Diana, C., Florin, C., Valentin, I. P., 2011. Amorphous cellulose–structure and characterization. Cellulose chemistry and technology Cellulose chem. Technol., 45 (1-2), 13-21.

17.Dan, C: Biocomposites reinforced with cellulose nanocrystals derived from potato peel waste. A Thesis Submitted to the School of Graduate Studies in Partial Fulfillment of the Requirements for the Degree Master of Applied Science McMaster University, Imperial College London, UK, 2011.

18.Francesca, L., Roberta, D. S., Donato, C., Giuseppe, V., Alfonso, M., 2012. Monitoring wood degradation during weathering by cellulose crystallinity. Taiwan. J. for Sci. 25 (3): 251- 64.

19.Filpponen, I: The synthetic strategies for unique properties in cellulose nanocrystals materials: A dissertation submitted to the Graduate Faculty of North Carolina State University In partial fulfillment of the Requirements for the degree of Doctor of Philosophy Wood & Paper Science Raleigh, North Carolina, 2009.

20.Gabriela, T. C., Daniella, L. M., Elisabete, F., Shirley, P., Omar, A. E. S., 2010. Some aspects of cetylation of untreated and mercerized sisal cellulose. J. Braz. Chem. Soc., 21, No. 1, 71-77.

21.Hassan, S., Ilari, F., Sarah, P. C., Dermot, F. B., Dimitris, S. A., 2011. Production of cellulose nanocrystals using hydrobromic acid and click reactions on their surface. J. Mater Sci. DOI 10.1007/s10853-011-5696-0

22.Haoran, W., Katia, R., Scott, R., Peter, J. V., 2014. Environmental science and engineering applications of nanocellulose-based nanocomposites (Review): Environ. Sci.: Nano, 1, 302–316: DOI: 10.1039/c4en00059e.

23.Jabbar, A. M., Timell, T. E., 1960. Isolation and characterization of cellulose from the inner bark of white birch (Betula Papyrifera). Can. J. Chem., 38, 1191-1198.

24.Juan, I. M., Vera, A. A., Viviana, P. C., Analia, V., 2008. Extraction of cellulose and preparation of nanocellulose from sisal fibers. Cellulose, 15, 149–159; DOI 10.1007/s10570-007-9145-9.

25.Jonas, B.: Investigation of Bacterial Cellulose as a Carbon Fiber Precursor and its Potential for Piezoelectric Energy Harvesting. A Thesis Presented to the Faculty of the Graduate School of Cornell University in Partial Fulfilment of the Requirements for the Degree of Master of Science, August, 2014.

26.Jering, A., Günther, J., 2010. Use of renewable raw materials with special emphasis on chemical industry. European Topic Centre on Sustainable Consumption and Production (ETC/SCP 2010), Højbro Plads 4; DK-1200 Copenhagen K, Website: http://scp.eionet.eu.int

27.Juergen, P., Steven, A. W., Dirk, H., 2011. Degradation of cellulose acetate-based materials (A review). J. Polym. Environ., 19, 152–165 DOI 10.1007/s10924-010-0258-0.

28.Joao, P. S. M., Morsyleide, D. F. R., Men, D. S. M. D. S. F.,

Lidyane, D. N., Diego, M. D. N., Ana, R. C., 2013. Extraction and characterization of nanocellulose structures from raw cotton Linter. Carbohydrate Polymers, 91, 229-235.

29.Kuga S., Brown R. M. Jr., 1987. Lattice imaging of ramie cellulose. Polymer Commun., 28, 311-314.

30.Lani, N. S., Ngadi, N., Johari, A., Jusoh, M., 2014. Isolation, characterization and applications of nanocellulose from oil palm empty fruit bunch fiber as nanocomposites. Journal of Nanomaterials, Volume 2014, Article ID 702538, 9 pages. http://dx.doi.org/10.1155/2014/702538.

31.Loo, M. M. L., Hashim, R., Leh, P. C., 2012. Recycling of a valueless paper dust to a Low Grade Cellulose Acetate: Effects of Pretreatment on Acetylation. Bioresources, 7(1), 1068-1083.

32.Marthin Hubbe A., Orlando R., Lucian Lucia A., Mohini S., 2008. Cellulosic nanocomposites-A Review. BioResources, 3 (3), 929-980.

33.Matheus, P., Heitor, L. O. J., Ademir, J. Z., 2014. Native Cellulose: Structure, Characterization and Thermal Properties. Materials, 7, 6105-6119; doi:10.3390/ma7096105.

34.Mayra, M., Lucimara, L. S., Nelson, D., Ljubica, T., 2015. Enhanced materials from nature: Nanocellulose from citrus waste. Molecules, 20, 5908-5923; doi:10.3390/molecules20045908.

35.Michael, T. P., Robert, J. M., Alan, W. R., Michael, A. B., 2013. Production and applications of cellulose nanomaterials. TAPPI PRESS 15 Technology Parkway South Suite 115 Peachtree Corners, GA 30092 U.S.A. www.tappi.org: ISBN: 978-1-59510-224-9.

36.Mizi, F., Dasong, D., Biao, H., 2012. Fourier transform infrared spectroscopy for natural fibres, fourier transform - Materials Analysis, Dr Salih Salih (Ed.), ISBN: 978-953-51-0594-7, InTech, http://www.intechopen.com/books/fourier-transform-materials-analysis/fourier-transform-infraredspectroscopy-for-natural-fibres.

37.Maria, E. V., Maria, S. P., Orlando, J. R., 2012. All-Cellulose Composite Fibers Obtained by Electrospinning Dispersions of Cellulose Acetate and Cellulose Nanocrystals. J. Polym Environ . 1-10; DOI 10.1007/s10924-012-0499-1.

38.Meiling, Y., Shujun, L., Mingxin, Z., Chunjie, L., Feng, D., Wei, L., 2013. Characterization of surface actylated nanocrystalline cellulose by single-step method. Bio-Resources, 8 (4), 6330-6341.

39.Nor, F. M. Z., Salma, M. Y., Ishak, A., 2014. Preparation and characterization of cellulose and nanocellulose from pomelo (citrus grandis) albedo. J. Nutr. Food Sci. 5 (1), 1-4 http://dx.doi.org/10.4172/2155-9600.1000334.

40.Narjes, K. M., Omid, R., Hossein, K., 2012. Production of Nanocrystalline Cellulose from Sugarcane Bagasse. Proceedings of the 4th International Conference on Nanostructures (ICNS4) 12-14 March, 2012, Kish Island, I.R. Iran.

41.Gabriel, A. O., The eight inaugural lecture 12th february, 2009. Journey to the promise land: The travails of an organic chemist. Department of Chemistry, Faculty of Science, University of Ilorin. Nigeria. Pp 17.

42.Peng B. L., Dhar N., Liu H. L., Tam K. C., 2011. Chemistry and Applications of Nanocrystalline Cellulose and its Derivatives: A Nanotechnology Perspective. Can. J. Chem. Eng. 9999:1–16: DOI 10.1002/cjce.20554.

43.Ping, L, You-Lo, H., 2012. Preparation and characterization of cellulose nanocrystals from rice straw. Carbohydrate Polymers, 87, 564– 573.

44.Paulo, H. F. P., Herman, C. J. V., Maria, O. H. C., Daniella, R. M., Sandra, M. D. L., Maria, L. C. P. D. S., 2011. Sugarcane baggasse pulping and bleaching: Thermal and chemical characterization. Bio-Resources, 6 (3), 2471-2481.

45.Poulami, B., Bonala, S. S., Kumar, U. N. Manjubala, I., 2014. Polymer ceramic composite for bone regeneration application. Int.J. ChemTech Res. 6(8), 4038-4041.

46.Qingqing, L., (2012). Nanocellulose: Preparation, characterization, supramolecular modeling, and its life cycle assessment. A Dissertation submitted to the Faculty of Virginia Polytechnic Institute and State University in Partial Fulfillment of the Requirements for the Degree of Doctor of Philosophy in Forest Products, Blacksburg, Virginia.

47.Rodionova, G., Lenes, M., Eriksen, O., Gregersen, O., Berichte, L., 2009. Surface chemical modification of microfibrillated cellulose: Improvement of barrier properties for packaging applications. 87, 38-46.

48.Rosa, M. F., Medeiros, E. S., Malmonge, J. A., Gregorski, K. S., Wood, D. F., Mattoso, L. H. C., Glenn, G., Orts, W. J., Imam, S. H., 2010. Cellulose nanowhiskers from coconut husk fibers: Effect of preparation conditions on their thermal and morphological behavior. Carbohydrate Polymers, 81, 83–92.

49.Robert, M. J., Ashlie, M., John, N., John, S. Jeff, Y., 2011. Cellulose nanomaterials review: structure, properties and nanocomposites. Chem. Soc. Rev., 40, 3941–3994.

50.Ricardo J. B. Pinto*, Márcia C. Neves, Carlos Pascoal Neto and Tito Trindade 2012.

51.Composites of Cellulose and Metal Nanoparticles. Nanocomposites - New Trends and

52.Developments, Intech.74-96; http://dx.doi.org/10.5772/50553

53.Sercer, M., Raos. P., Rujnic-Sokele. M,: Processing of Wood-Thermoplastic Composites, www.jobwerks.com/news/Archives/iwpc.pdf

54.Saxena, A: Nanocomposites based on nanocellulose whiskers. A Dissertation Presented to The Academic Faculty In Partial Fulfillment of the Requirements for the Degree Doctor of Philosophy in the School of Chemistry and Biochemistry, Georgia Institute of Technology, May, 2013.

55.Stephen, J. E., 2010. Cellulose nanowhiskers: Promising materials for advanced applications. DOI: 10.1039/c0sm00142b

56.Saska, S., Barud, H. S., Gaspar, M. M. M., Marchetto, R., Ribeiro, S. J. L., Messaddeq, Y., 2011. Bacterial cellulose-hydroxyapatite nanocomposites for bone regeneration. International Journal of Biomaterials, 2011, Article ID 175362, 8 pages; doi:10.1155/2011/175362.

57.Tsegaye, G. A., 2012. Exploring potential environmental applications of selenium nanoparticles. Thesis submitted in partial

fulfilment of the requirements for the joint academic degree of International Master Of Science In Environmental Technology and Engineering, Ghent University (Belgium), Ictp (Czech Republic), Unesco-Ihe (The Netherlands).

58.Teboho, C. M., 2012. Preparation and Characterization of Vinyl Silane Cross-linked Thermoplastic Composites Filled with Natural Fibres.

59.Vigneshwaran, S., Prasad, S., 2011. Preparation of Spherical Nanocellulose by Anaerobic Microbial Consortium. 2nd International Conference on Biotechnology and Food Science, IPCBEE vol. 7, IACSIT Press, Singapore.

60.Vipul, S. C., swapan, k. C., 2012. Use of nanotechnology for high performance cellulosic and papermaking products, Cellulose chem. Technol., 46 (5-6), 389-400.

61.Xu, H., Wei-Dong, Z., 2010. Preparation of Cellulose Sulphate and Evaluation of its Properties. Journal of Fiber Bioengineering and Informatics, 3 (1) doi:10.3993/jfbi06201006 .

62.Xuezhu, X., Fei, L., Long, J., Zhu, J. Y., Darrin, H., Dennis, P. W., 2013. Cellulose Nanocrystals vs. Cellulose Nanofibrils: A Comparative Study on Their Microstructures and Effects as Polymer Reinforcing Agents. ACS Appl. Mater. Interfaces, 5, 2999−3009.

63.Xiaolin, Y., Shengrui, T., Maofa, G., Lingyan, W., Junchao, Z., Changyan, C., Weiguo, S., 2012. Adsorption of heavy metal ions from aqueous solution by carboxylated cellulose nanocrystals. Journal of Environmental Sciences, 24, 1-26; DOI: 10.1016/S1001-0742(12)60145-4.

64.Youssef, H., Henri, C., Michel, R. V., 2006. TEMPO-mediated surface oxidation of cellulose whiskers. Cellulose, 13, 679 –687; DOI 10.1007/s10570-006-9075-y.

65.Yakubu, A., Olatunji, G. A., Sunday, O., Olubunmi, A., 2012. Ketene acetylated wood cellulose for industrial applications in wood-base and polymer industry. Journal of Environmental Science and Technology, 5 (3), 168–176.

66.Yanxia, Z., Tiina, N., Carlos, S., Julio, A., Ingrid, C. H., Orlando, J. R., 2013. Cellulose Nanofi brils: From Strong Materials to Bioactive Surfaces. J. Renew. Mater., 1(3), 195-211: DOI: 10.7569/JRM.2013.634115.

67.Yiying, Y., 2011. A Comparative Study of Cellulose I and II Fibers and Nanocrystals. A Thesis Submitted to the Graduate Faculty of the Louisiana State University and Agricultural and Mechanical College in Partial Fulfilment of the Requirements for the degree of Master of Science in The School of Renewable Natural Resources.

68. 68. Yucheng, P., Douglas, J. G., Yousoo, H., Alper, K., Zhiyong, Cai. And Mandla, A. T., 2013. Influence of drying method on the material properties of nanocellulose I: Thermostability and crystallinity. Cellulose, 1-14: DOI 10.10071s10570-013-0019-z.

69. Zhang, Z., 2013. Chemical functionalization of nano brillated cellulose by alkoxysilanes: Application to the elaboration of composites and foams. Universite Sciences et Technologies -Bordeaux I, 2013. English <NNT: 2013BOR14888>. <tel-00952026>.

70. Zhao, Y., Sugiyama, S., Miller, T., & Miao, X., (2008). Nanoceramics for blood-borne virus removal. Expert Review of Medical Devices, 5(3), 395 - 405.

Appendices

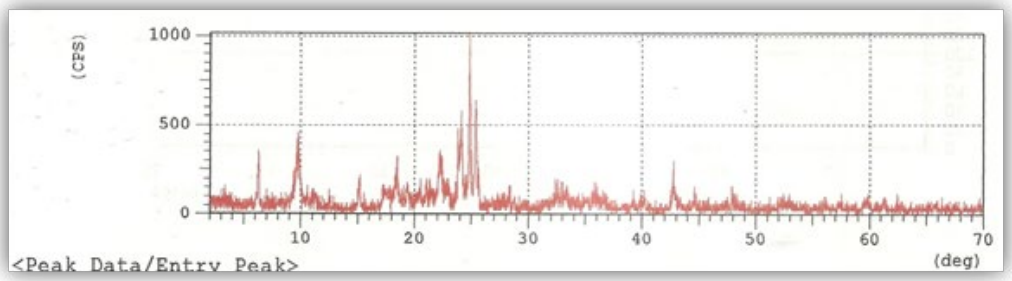

Appendix A: AZEH3-CELL-3h-HC1

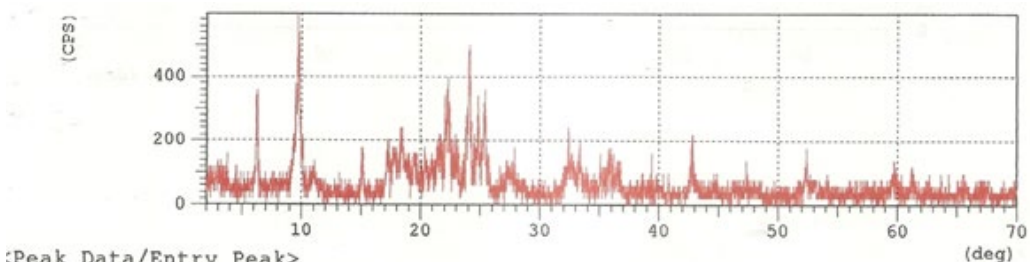

Appendix B: AZEH4-CA-3h-HCl

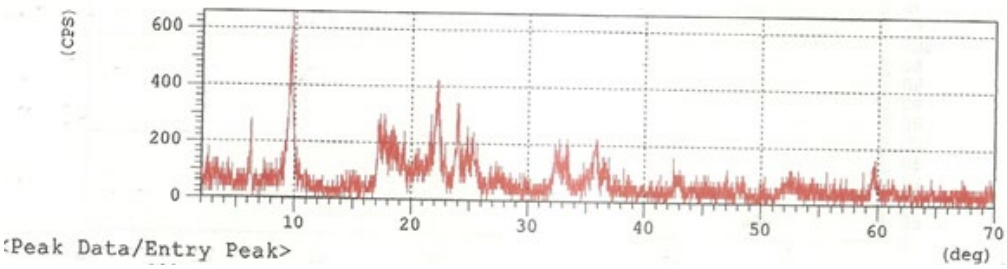

Appendix C: AZEH7-CELL-3h-H3PO4

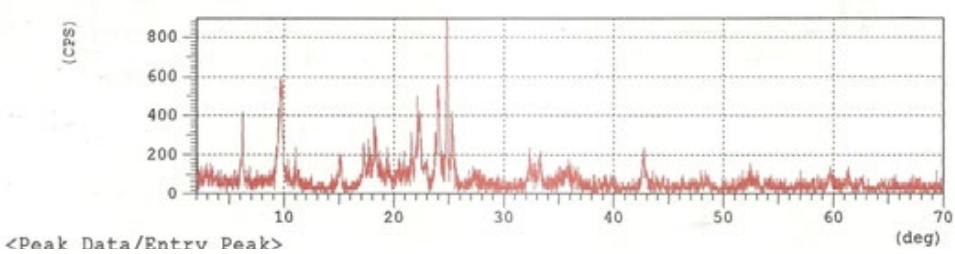

Appendix D: AZEH 8-CA-H3PO4

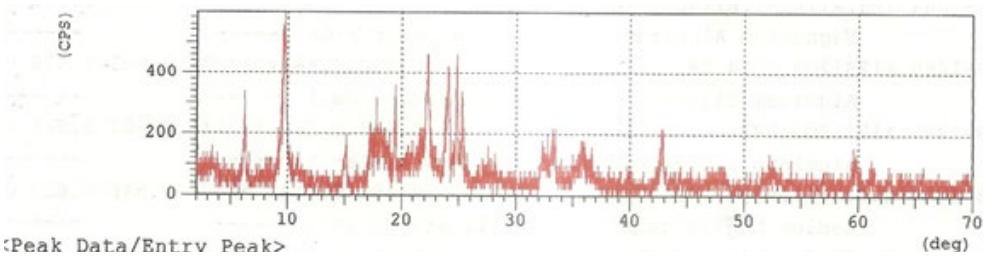

Appendix E: AZEH10-CELL-6h-H3PO4

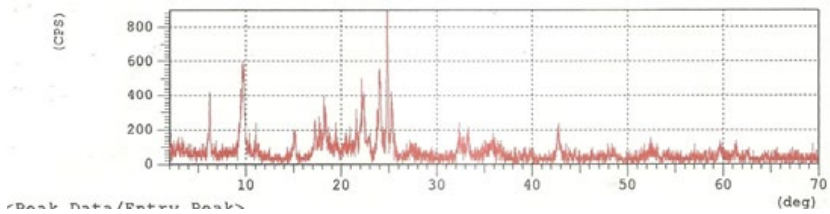

Appendix F: AZEH 11-CA-6h-H3PO4

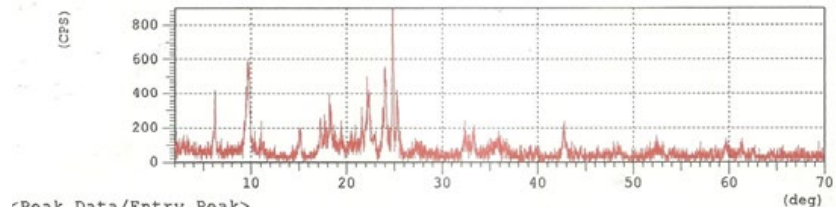

Appendix G: AZEH12-MC-1h-H3PO4

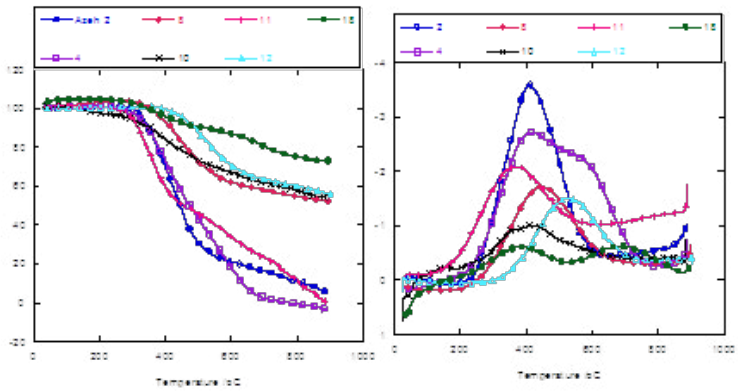

Appendix H: TGA and DTG Curves of the nanoparticles studied